Resonance Raman, Infrared, and Normal Coordinate Analysis of Free-Base Tetraphenylbacteriochlorin: A Model for Bacteriopheophytins

Ching-Yao Lin and Thomas G. Spiro*

Department of Chemistry, Princeton University, Princeton, New Jersey 08544

Received: August 14, 1996; In Final Form: October 25, 1996[⊗]

Resonance Raman (RR) and FT-IR spectra are reported for free-base tetraphenylbacteriochlorin and its pyrrole-$^{15}N_4$, β-D_8, *meso*-$^{13}C_4$, and phenyl-D_{20} isotopomers. A normal mode analysis is carried out in order to assign observed RR and IR modes, using a NiTPP-based force field, with bond-distance scaling of force constants and the introduction of long-range interaction constants. The modes correlate well with those of NiTPP, once due allowance is made for direct effects of pyrrole ring reduction: inequivalent $C_\beta-C_\beta$ and $C_\alpha-C_\beta$ bonds and extra $C_\beta-H$ bending modes. Although the $C_\alpha-C_m$ and $C_\alpha-N$ bonds of the 16-membered inner ring are not strictly equivalent, there is little tendency for mode localization with respect to these bonds. The absence of a central metal lowers the frequencies of $C_\alpha-C_m$ stretching and pyrrole translational modes. The RR enhancement pattern is quite different than for porphyrins. Totally symmetric modes dominate spectra in resonance with the Q_x band, due to a larger transition moment than in porphyrins, while non-totally symmetric modes are strongly enhanced in the region of the close-lying B_x and B_y transitions, reflecting vibronic coupling between them.

Introduction

Bacteriochlorophylls (BChl) and bacteriopheophytins (BPh) play important roles in light harvesting, energy transduction, and charge separation in the purple bacteria.[1,2] Crystal structures of photosynthetic reaction center complexes have been reported,[3−5] and spectroscopic techniques are providing a detailed understanding of the electronic and molecular structure of these tetrahydroporphyrin derivatives and their interactions with the protein hosts. EPR, ENDOR, and TRIPLE have been used to study the radical species within the chromatophore,[6,7] and FT-IR spectra have also been reported for the anion radicals of bacteriochlorophylls.[8] Resonance Raman (RR)[9] and FT-Raman[10] spectroscopies have been employed because of their sensitivity and selective enhancement for vibrational modes of the chromophores.[11−13]

Interpretation of the Raman spectra is hampered by their complexity and by incomplete analysis of the vibrational modes. There is good understanding of the vibrational modes of porphyrins, thanks to extensive experimental and computational studies of many derivatives and isotopomers, and this analytical framework is being extended to hydroporphyrins, including chlorins,[14−19] isobacteriochlorins,[20−22] and bacteriochlorins.[18b,23] The bacteriochlorin normal mode studies have focused on nickel 1,5-dihydroxy-1,5-dimethyloctaethylbacteriochlorin [Ni(HOEBC)][23] and copper tetraphenylbacteriochlorin (CuTPBC).[18b] We now report a comprehensive study of free-base tetraphenylbacteriochlorin (H_2TPBC, Figure 1) including IR and variable wavelength RR spectra of four isotopomers: [*pyrrole*-$^{15}N_4$]-, [β-D_8]-, [*meso*-$^{13}C_4$]-, and [*phenyl*-D_{20}]H_2TPBC. Assignments are made with the aid of a normal coordinate analysis, and the extensive data permit the development of a high-quality force field. Because the analysis is for a bacteriochlorin free-base, the results are expected to be useful in interpreting RR studies of the bacteriopheophytin primary acceptor in reaction centers.[1−5]

Experimental Section

Synthesis. H_2TPBC was prepared from H_2TPP (Mid-Century, Posen, IL) according to the methods of Whitlock *et al.*[24] However, we found that using excess reducing agent (3 g of toluenesulfonylhydrazine to 200 mg of H_2TPP) dramatically shortened the reaction time from the reported 6.5 h to less than half an hour.

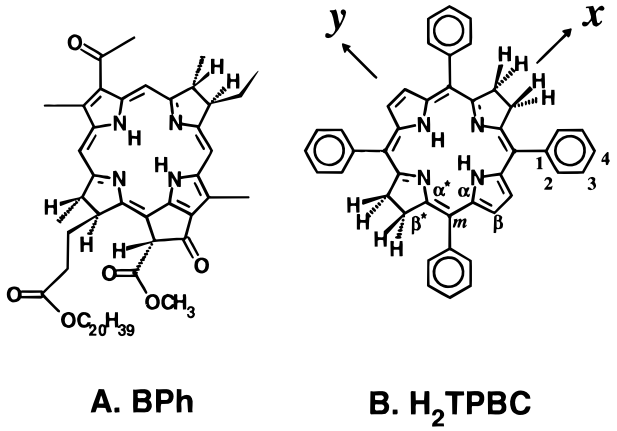

Figure 1. Molecular structures of (a) bacteriopheophytin *a* (BPh) and (b) free-base tetraphenylbacteriochlorin (H_2TPBC). Atom labels are shown for H_2TPBC.

Free-base [*pyrrole*-$^{15}N_4$]-, [β-D_8]-, [*meso*-$^{13}C_4$]-, and [*phenyl*-D_{20}]TPBC were obtained from the respective porphyrin isotopomers, which were prepared from isotope-labeled pyrroles (D_5 and ^{15}N) and benzaldehydes (D_5 and ^{13}C) according to the method of Lindsey *et al.*[25] Deuterated H_2TPBCs (D_8 and D_{20}) were checked by NMR spectroscopy to ensure the quality of isotope labeling.

Spectroscopy. Resonance Raman spectra were obtained in backscattering geometry either from THF solution in a spinning NMR tube or from a rotating KBr pellet under vacuum. Excitation lines were provided with a Coherent Innova 100K3 krypton ion laser (520.8 nm) and a Spectra-Physics 2025 argon ion laser (363.8 nm). The scattered light was collected and dispersed with a Spex 1404 double monochromator equipped with a cooled photomultiplier (RCA 31034A-02). To minimize laser-induced degradation, solutions were prepared with freshly distilled THF, which was vigorously degassed with at least three freeze−pump−thaw cycles.

* To whom correspondence should be addressed.

[⊗] Abstract published in *Advance ACS Abstracts,* December 15, 1996.

S1089-5647(96)02479-0 CCC: $14.00

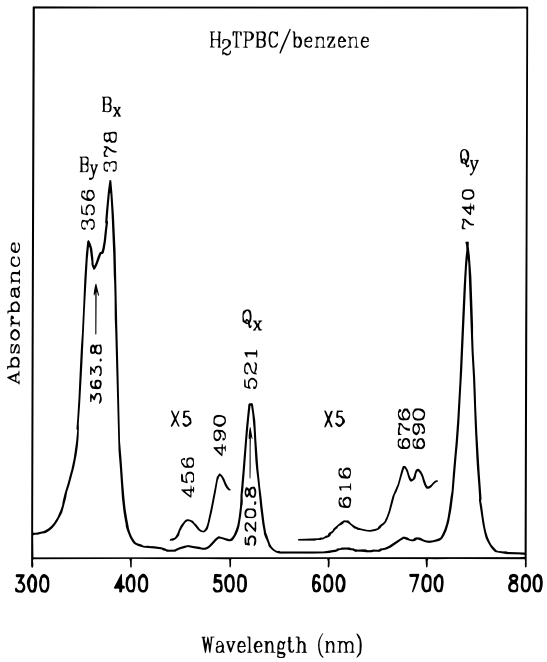

Figure 2. UV−vis spectrum of H_2TPBC in benzene. The arrows indicate the positions of excitation laser lines in the RR experiments.

The electronic absorption spectrum was obtained with a 1-cm quartz cell on a Hewlett-Packard 8452A diode array spectrophotometer. The FT-IR spectra of H_2TPBC were recorded on a Nicolet 730 Fourier transform infrared (FT-IR) spectrophotometer. All the spectral data were imported into and processed with Labcalc software (Galactic Industries Co., Salem, NH).

Normal Coordinate Analysis (NCA). Normal mode calculations were performed with the empirical **GF** matrix method of Wilson.[26] The molecular geometry was taken from the crystal structure of five-coordinated zinc tetraphenylbacteriochlorin[27] and slightly modified to retain D_{2h} symmetry. The internal coordinates are Wilson-type bond-stretching and angle-bending coordinates. The symmetry coordinates ($\mathbf{S}_i$) and the corresponding **U** matrix were obtained from symmetry-adapted linear combination of internal coordinates. A menu-driven, graphically interfaced version of Schachtschneider's program, developed in our laboratory and implemented on a R3000 Indigo workstation (Silicon Graphics Inc.),[28] was used to set up the **G** matrix and to solve the secular equation $|\mathbf{GF} - \mathbf{E}\lambda| = 0$.

Results and Discussion

A. Electronic Structure. The UV−vis absorption spectrum of H_2TPBC (Figure 2) resembles those of bacteriochlorins and bacteriopheophytins[1,6a,b] and differs from those of porphyrins[29] in having a split Soret band (356 and 378 nm, B_y and B_x) and two strong Q bands (521 and 740 nm, Q_x and Q_y). The Q_y band is as strong as the Soret bands, while the Q_x band has nearly half of the Soret band intensity. These features can be understood on the basis of Gouterman's four-orbital model for porphyrins and their derivatives.[29] For D_{4h} metalloporphyrins, the two degenerate lowest unoccupied molecular orbitals (LUMO, e_g*) and two nearly degenerate highest occupied molecular orbitals (HOMO, a_{1u} and a_{2u}) give rise to a strong Soret band in the near-UV region and weak Q bands in the visible region, as a result of configuration interactions. This interaction is lifted in H_2TPBC (Figure 3) because of the reduction of two opposite pyrrole rings. The degenerate e_g* (D_{4h}) LUMOs split into *x* and *y* components (b_{3g} and b_{2g}, under D_{2h}). The b_{3g} and a_u orbitals are more destabilized relative to the b_{2g} and b_{1u} orbitals because of their orbital nodal pattern.[29] As a result, the two *y* polarized electronic transitions ($a_u \times b_{2g} = b_{2u}$ and $b_{1u} \times b_{3g} = b_{2u}$, under D_{2h} symmetry) are energetically well separated, and the lowest (Q_y) and highest (B_y) energy absorption bands have nearly equal intensity. The two *x* polarized transitions ($a_u \times b_{3g} = b_{3u}$ and $b_{1u} \times b_{2g} = b_{3u}$) are sufficiently close in energy to experience some configuration interactions, leaving the Q_x band with half the intensity of the B_x band.

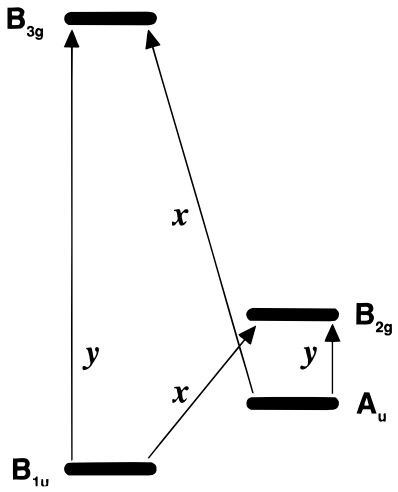

Figure 3. Frontier orbitals of bacteriochlorins.

TABLE 1: Structure Parameters Used[a] in Normal-Coordinate Analysis of H_2TPBC

Bacteriochlorin Core		
	pyrrole rings	pyrroline rings
Bond Length, Å		
$C_\beta-C_\beta$	1.366	1.488
$C_\alpha-C_m$	1.404	1.384
$C_\alpha-C_\beta$	1.447	1.493
$C_\alpha-N$	1.378	1.371
$C_\beta-H$	1.087	1.088
N−H	0.997	
C_1-C_m	1.500	
Bond Angle, deg		
$C_\alpha-C_m-C_\alpha$	119.2	
$C_\alpha-C_\beta-C_\beta$	106.3	103.5
$C_\alpha-N-C_\alpha$	104.6	105.7
$C_\beta-C_\alpha-C_m$	121.0	118.1
$C_\beta-C_\alpha-N$	111.4	113.6
$C_m-C_\alpha-N$	127.7	128.3
$C_\alpha-C_m-C_1$	120.0	120.9
$C_\alpha-C_\beta-H$	128.7	112.5
$C_\beta-C_\beta-H$	125.0	109.2
$C_\alpha-N-H$	127.7	
$H-C_\beta-H$		109.7

Phenyl Substituents			
Bond Length, Å		Bond Angle, deg	
C_1-C_2	1.372	$C_1-C_2-C_3$	119.4
C_2-C_3	1.390	$C_2-C_1-C_2$	121.1
C_3-C_4	1.361	$C_2-C_3-C_4$	118.6
C_p-H_p	1.100	$C_3-C_4-C_3$	122.8
		$C_m-C_1-C_2$	119.4
		$C_1-C_2-H_p$	120.6
		$C_3-C_4-H_p$	120.2
		$C_2-C_3-H_p$	119.8

[a] Taken from ref 28.

B. Normal Coordinate Analysis. A planar model was employed to carry out the normal mode calculation in order to avoid the mixing of in-plane and out-of-plane vibrations and to keep the number of calculated frequencies tractable. The structure parameters used in the normal coordinate analysis were taken from the crystal structure of (Py)ZnTPBC[27] (Table 1). We note that the phenyl C−C bonds have different lengths

TABLE 2: Valence Force Constants for H_2TPBC

Bacteriochlorin Core

	pyrrole	pyrroline		pyrrole	pyrroline
Stretch, mdyn/Å					
K($C_\beta C_\beta$)	7.350	3.900	K(C_βH)	5.200	4.600
K($C_\alpha C_m$)	6.500	6.900	K(NH)	6.300	
K(C_αN)	5.700	5.800	K(C_1C_m)	4.900	
K($C_\alpha C_\beta$)	5.020	4.300			
Bend, mdyn/rad²					
H($C_1C_mC_\alpha$)	0.900	1.100	H($C_\beta C_\alpha$N)	1.400	1.200
H($C_\alpha C_\beta C_\beta$)	1.370	1.200	H($C_\beta C_\beta$H)	0.440	0.694
H(C_αNC_α)	1.600	1.750	H($C_\alpha C_\beta$H)	0.400	0.716
H(C_mC_αN)	1.000	1.100	H(HC_βH)		0.475
H($C_\beta C_\alpha C_m$)	0.730	0.630	H(C_αNH)	0.275	
H($C_\alpha C_m C_\alpha$)	1.250				
1,2 Stretch Stretch Interactions, mdyn/Å					
($C_\alpha C_m$)(C_1C_m)	0.308	0.420	(C_αN)(C_αN)	0.432	0.595
($C_\alpha C_m$)($C_\alpha C_\beta$)	0.628	0.300	($C_\beta C_\beta$)($C_\alpha C_\beta$)	0.600	0.316
(C_αN)($C_\alpha C_\beta$)	0.480	0.314	($C_\alpha C_m$)($C_\alpha C_m$)	0.422	
(C_αN)($C_\alpha C_m$)	0.653	0.680			
Stretch Bend Interactions (Two Atoms Common), mdyn/rad					
(C_1C_m)($C_1C_mC_\alpha$)	0.150	0.150	(C_αN)(C_αNC_α)	0.250	0.320
($C_\alpha C_m$)($C_1C_mC_\alpha$)	0.090	0.100	(C_αN)($C_\beta C_\alpha$N)	0.300	0.300
($C_\alpha C_\beta$)($C_\alpha C_\beta C_\beta$)	0.220	0.070	(C_αN)(C_mC_αN)	0.290	0.320
($C_\alpha C_\beta$)($C_\beta C_\alpha C_m$)	0.220	0.150	($C_\beta C_\beta$)($C_\alpha C_\beta C_\beta$)	0.200	0.100
($C_\alpha C_\beta$)($C_\beta C_\alpha$N)	0.230	0.150	($C_\alpha C_\beta$)($C_\alpha C_\beta$H)	0.072	0.160
($C_\alpha C_m$)($C_\alpha C_mC_\alpha$)	0.190	0.200	($C_\beta C_\beta$)($C_\beta C_\beta$H)	0.090	0.224
($C_\alpha C_m$)($C_\beta C_\alpha C_m$)	0.180	0.150	(C_αN)(C_αNH)	0.050	
($C_\alpha C_m$)(C_mC_αN)	0.180	0.220			
Stretch Bend Interactions (One Atom Common:Central), mdyn/rad					
($C_\alpha C_\beta$)(C_mC_αN)	−0.230	−0.200	($C_\beta C_\beta$)($C_\alpha C_\beta$H)	−0.080	
($C_\alpha C_m$)($C_\beta C_\alpha$N)	−0.220	−0.230	($C_\alpha C_\beta$)($C_\beta C_\beta$H)	−0.020	
(C_αN)($C_\beta C_\alpha C_m$)	−0.230	−0.240	(C_1C_m)($C_\alpha C_mC_\alpha$)	−0.300	
($C_\alpha C_m$)($C_1C_mC_\alpha$)	−0.090	−0.100			
Stretch Bend Interactions (One Atom Common:Side), mdyn/rad					
($C_\alpha C_\beta$)(C_αNC_α)	−0.115	−0.100	(C_αN)($C_\beta C_\alpha$N)	−0.115	−0.115
(C_αN)($C_\alpha C_\beta C_\beta$)	−0.115	−0.110	(C_αN)(C_mC_αN)	−0.115	−0.130
(C_αN)($C_\alpha C_mC_\alpha$)	−0.120	−0.130	($C_\alpha C_\beta$)($C_\beta C_\beta$H)	−0.079	
Bend Bend Interactions (Two Atoms Common), mdyn/rad²					
($C_\alpha C_mC_\alpha$)($C_1C_mC_\alpha$)	0.090	0.090	($C_\alpha C_\beta$H)($C_\alpha C_\beta C_\beta$)		0.020
($C_\beta C_\alpha$N)($C_\beta C_\alpha C_m$)	0.040	0.020	($C_\beta C_\beta$H)($C_\alpha C_\beta$H)		0.025
(C_mC_αN)($C_\beta C_\alpha C_m$)	0.030	0.020	($C_\beta C_\beta$H)($C_\beta C_\beta$H)		−0.028
(C_mC_αN)($C_\beta C_\alpha$N)	0.030	0.020			
1,3 Stretch Stretch Interactions, mdyn/Å					
($C_\alpha C_\beta$)($C_\alpha C_\beta$)	0.456	0.180	($C_\alpha C_m$)($C_\beta C_\beta$)	−0.300	−0.111
($C_\alpha C_\beta$)(C_αN)	0.290	0.270	(C_αN)($C_\alpha C_m$)	−0.148	−0.168
(C_αN)($C_\beta C_\beta$)	0.172	0.083	($C_\alpha C_m$)($C_\alpha C_\beta$)	−0.034	−0.173
($C_\alpha C_m$)(C_αN)	−0.150	−0.100			
Other Stretch Stretch Interactions, mdyn/Å					
1,4 ($C_\alpha C_m$)($C_\alpha C_m$)	−0.041	−0.059	1,6 ($C_\alpha C_m$)($C_\alpha C_m$)	−0.068	−0.117
1,4 ($C_\beta C_\beta$) ($C_\alpha C_m$)	0.100		1,9 ($C_\alpha C_m$)($C_\alpha C_m$)	−0.052	−0.021
1,5 ($C_\alpha C_m$)($C_\alpha C_m$)	0.057	0.132			

Phenyl Substituents

Stretch, mdyn/Å		1,2 Stretch Stretch Interactions, mdyn/Å		Stretch Bend Interactions (Two Atoms Common)	
K(C_1C_2)	6.220	(C_1C_2)(C_1C_m)	0.150	(C_1C_m)($C_mC_1C_2$)	0.250
K(C_2C_3)	6.200	(C_1C_2)(C_1C_2)	0.770	(C_1C_2)($C_mC_1C_2$)	0.108
K(C_3C_4)	6.300	(C_2C_3)(C_1C_2)	0.770	(C_1C_2)($C_1C_2H_p$)	0.275
K(C_pH_p)	5.116	(C_2C_3)(C_3C_4)	0.770	(C_2C_3)($C_pC_pH_p$)	0.210
Bend, mdyn/rad²		(C_3C_4)(C_3C_4)	0.800	(C_3C_4)($C_pC_pH_p$)	0.335
H($C_mC_1C_2$)	0.755	**Other Stretch Stretch Interactions, mdyn/Å**		**Stretch Bend Interactions (One Atom Common)**	
H($C_pC_pC_p$)	0.970	1,3 (C_pC_p)(C_pC_p)	−0.300	(C_1C_m)($C_2C_1C_2$)	−0.300
H($C_1C_2H_p$)[a]	0.525	1,4 (C_1C_2)(C_3C_4)	0.250		
H($C_2C_3H_p$)[a]	0.565	1,4 (C_2C_3)(C_2C_3)	0.320		
H($C_3C_4H_p$)[a]	0.450				

[a] H($C_xC_yH_p$) = H($C_yC_xH_p$).

(1.361, 1.372, and 1.390 Å, a feature also seen in biphenyl[30,31]). We found it necessary to use different force constants as well as bond lengths for these bonds in order to reproduce the phenyl vibrational frequencies.

The starting point of the calculation was the force field developed for NiTPP[32], with the addition of N−H bending force constants taken from free-base porphine.[33] The C−C and C−N stretching force constants were scaled to the bond distances using the equation of Burgi−Dunitz.[34] The bending force constants and the stretch−stretch interaction terms were adjusted in parallel with the changes made to the stretching force constants. Slight alterations were made to improve the fit to

TABLE 3: Observed and Calculated Skeletal Mode Frequencies (cm^{-1}) for H_2TPBC[a]

	obsd					calcd					
mode	N.A.	$\Delta^{15}N$	$\Delta^{13}C$	ΔD_8	ΔD_{20}	N.A.	$\Delta^{15}N$	$\Delta^{13}C$	ΔD_{12}	ΔD_{20}	assignment (PED, %)
						A_g Skeletal Modes					
ν_{N-H}						3383	9	0	0	0	99% ν(N−H)
ν_5						3099	0	0	778	0	98% $\nu(C_\beta-H)$
ν_{14}						2870	0	0	762	0	99% $\nu(C_\beta-H)$*
ν_{10}	1565	2	18	14	0	1568	0	20	8	0	50% $\nu(C_\alpha C_m)$*, 18% $\nu(C_\alpha C_m)$, 14% $\nu(C_\beta C_\beta)$, 6% $\nu(C_\alpha C_\beta)$*
ν_2	1521	1	11	10	2	1521	1	13	8	3	42% $\nu(C_\alpha C_m)$, 13% $\nu(C_\beta C_\beta)$, 8% $\nu(C_\alpha C_\beta)$, 8% $\nu(C_1C_m)$, 7% $\delta(C_\beta C_\alpha N)$
ν_3				(1402)		1444	0	7	0	−5	35% $\delta(HC_\beta H)$*, 17% $\nu(C_\alpha C_m)$*, 10% $\nu(C_\beta C_\beta)$, 7% $\delta(C_\alpha C_\beta H)$*
ν_4	1367	14	3	20	9	1368	7	3	7	5	18% $\nu(C_\alpha C_\beta)$, 17% $\nu(C_\alpha C_\beta)$*, 16% $\nu(C_\alpha N)$*, 10% $\delta(C_mC_\alpha N)$*, 10% $\delta(C_\alpha NC_\alpha)$*
ν_{12}	1297	7	1	4	1	1300	10	0	9	0	31% $\nu(C_\alpha N)$, 29% $\nu(C_\alpha N)$*, 12% $\nu(C_\alpha C_\beta)$, 6% $\delta(C_mC_\alpha N)$
ν_1	1226	9	10	−7	50	1225	2	4	−5	50	32% $\nu(C_1C_m)$, 15% $\delta(C_2C_3H_p)$, 9% $\nu(C_\alpha N)$, 7% $\nu(C_\alpha N)$*, 6% $\delta(C_1C_2H_p)$
ν_9	1076	0	0	307	1	1074	0	1	308	3	39% $\delta(C_\beta C_\beta H)$, 30% $\delta(C_\alpha C_\beta H)$, 8% $\nu(C_\beta C_\beta)$
ν_{11}	1026	0	0	−155	2	1028	2	3	−124	0	23% $\nu(C_\beta C_\beta)$*, 10% $\delta(C_\beta C_\beta H)$*, 9% $\nu(C_\alpha C_\beta)$, 8% $\nu(C_\alpha N)$
ν_6	995	8	2	13	0	983	5	2	−3	0	23% $\nu(C_\beta C_\beta)$*, 21% $\nu(C_\alpha C_\beta)$, 7% $\nu(C_\alpha N)$, 6% $\nu(C_\alpha C_\beta)$*
ν_{15}	968	9	3		1	948	6	8	30	9	22% $\nu(C_\alpha C_\beta)$*, 15% $\nu(C_\alpha N)$*, 11% $\nu(C_1C_2)$
ν_7	856	4	6	31	1	862	4	6	23	−2	26% $\nu(C_\alpha C_\beta)$*, 8% $\delta(C_\beta C_\alpha N)$, 8% $\nu(C_\alpha C_\beta)$, 8% $\nu(C_1C_2)$, 6% $\delta(C_\alpha NC_\alpha)$
ν_{16}	822	7	5	−31	12	814	8	9	−16	−2	15% $\delta(C_\alpha NC_\alpha)$*, 15% $\nu(C_\beta C_\beta)$*, 12% $\delta(C_1C_mC_\alpha)$*, 10% $\delta(C_1C_mC_\alpha)$
ν_8	335	4	2	9	3	330	2	0	7	2	23% $\delta(C_\alpha C_mC_\alpha)$, 10% $\delta(C_1C_mC_\alpha)$*
ν_{13}						298	0	0	0	0	31% $\delta(C_1C_mC_\alpha)$, 26% $\delta(C_1C_mC_\alpha)$*, 7% $\nu(C_\alpha C_m)$*
ν_{18}	166	0	0	3	2	157	1	0	3	0	25% $\delta(C_mC_\alpha N)$*, 24% $\delta(C_mC_\alpha N)$, 16% $\delta(C_\beta C_\alpha C_m)$, 15% $\delta(C_\beta C_\alpha C_m)$*
						B_{1g} Skeletal Modes					
ν_{23}						3095	0	0	788	0	98% $\nu(C_\beta-H)$
ν_{31}						2869	0	0	761	0	99% $\nu(C_\beta-H)$*
ν_{19}	1560	4	20	0	0	1561	1	32	2	1	48% $\nu(C_\alpha C_m)$*, 43% $\nu(C_\alpha C_m)$
ν_{28}	1421	2	19	7	−5	1421	2	12	5	−14	27% $\nu(C_\alpha C_m)$*, 20% $\nu(C_\alpha C_m)$, 16% $\nu(C_\alpha N)$, 11% $\nu(C_1C_m)$, 10% $\nu(C_\alpha N)$*
ν_{29}	1381	1	5	127	7	1379	0	1	75	2	44% $\nu(C_\alpha C_\beta)$, 29% $\delta(C_\beta C_\beta H)$, 11% $\delta(C_\alpha C_\beta H)$, 11% $\delta(C_\alpha C_\beta C_\beta)$, 7% $\nu(C_\alpha N)$
ν_{27}	1320	10	12	0	14	1314	13	13	−2	17	35% $\nu(C_\alpha N)$, 23% $\nu(C_1C_m)$, 10% $\delta(C_\alpha NH)$, 6% $\delta(C_2C_3H_p)$
ν_{20}	1267	10	3	−9	18	1272	12	4	−19	16	64% $\nu(C_\alpha N)$*, 8% $\nu(C_\alpha C_\beta)$*, 7% $\nu(C_1C_m)$
ν_{34}						1146	1	1	346	0	15% $\delta(C_\beta C_\beta H)$, 15% $\delta(C_\alpha C_\beta H)$, 15% $\nu(C_\alpha C_\beta)$, 13% $\nu(C_\alpha C_\beta)$*, 8% $\nu(C_\alpha C_m)$
ν_{22}						1023	5	3	−172	11	11% $\delta(C_1C_2C_3)$, 10% $\delta(C_2C_3C_4)$, 9% $\nu(C_\alpha N)$*, 8% $\delta(C_\alpha NH)$, 6% $\nu(C_\alpha C_\beta)$*
ν_{30}						893	2	3	−84	1	34% $\delta(C_\alpha NH)$, 13% $\nu(C_\alpha C_\beta)$, 9% $\nu(C_\alpha N)$, 8% $\nu(C_\alpha C_\beta)$*
ν_{32}						865	4	2	44	1	30% $\delta(C_\alpha C_\beta C_\beta)$, 22% $\nu(C_\alpha N)$, 7% $\delta(C_\alpha C_\beta H)$, 6% $\delta(C_\alpha C_\beta C_\beta)$*
ν_{24}	738	0	3	63	−6	735	1	4	30	1	27% $\delta(C_\alpha C_\beta C_\beta)$*, 13% $\delta(C_\beta C_\alpha N)$*, 9% $\nu(C_\alpha C_\beta)$, 7% $\delta(C_\beta C_\alpha N)$, 6% $\nu(C_\alpha N)$*
ν_{25}						538	6	0	16	0	18% $\delta(C_1C_mC_\alpha)$*, 16% $\delta(C_1C_mC_\alpha)$, 13% $\delta(C_mC_\alpha N)$*, 13% $\delta(C_mC_\alpha N)$
ν_{35}						377	0	0	33	0	11% $\nu(C_\alpha C_m)$, 9% $\nu(C_\alpha C_m)$*, 7% $\delta(C_\beta C_\alpha N)$*, 6% $\delta(C_\beta C_\alpha C_m)$, 6% $\nu(C_\alpha C_\beta)$*
ν_{33}						376	2	1	2	6	17% $\nu(C_1C_m)$, 10% $\delta(C_mC_\alpha N)$, 10% $\delta(C_\beta C_\alpha C_m)$, 9% $\delta(C_2C_1C_2)$
ν_{21}	317	1	0	11	5	308	0	0	13	0	20% $\delta(C_1C_mC_\alpha)$*, 20% $\delta(C_1C_mC_\alpha)$, 18% $\delta(C_\beta C_\alpha C_m)$*, 17% $\delta(C_mC_\alpha N)$*
						B_{2u} Skeletal Modes					
ν_{43y}						3095	0	0	788	0	98% $\nu(C_\beta-H)$
ν_{45y}						2870	0	0	762	0	99% $\nu(C_\beta-H)$*
ν_{37y}	1581	2	18	1	−2	1581	0	24	3	0	64% $\nu(C_\alpha C_m)$*, 17% $\nu(C_\alpha C_m)$, 8% $\nu(C_\alpha C_\beta)$*
ν_{39y}	1460		9			1446	1	8	−10	−6	34% $\delta(HC_\beta H)$*, 14% $\nu(C_\alpha C_m)$, 9% $\nu(C_\alpha C_m)$*, 7% $\delta(C_\alpha C_\beta H)$*, 7% $\nu(C_\alpha N)$
ν_{40y}	1381	0	6	58		1382	1	1	73	5	41% $\nu(C_\alpha C_\beta)$, 27% $\delta(C_\beta C_\beta H)$, 12% $\delta(C_\alpha C_\beta H)$, 6% $\delta(C_\alpha C_\beta C_\beta)$
ν_{41y}	1365	7	2	5	3	1357	14	3	−2	7	32% $\nu(C_\alpha N)$, 19% $\nu(C_\alpha N)$*, 11% $\nu(C_\alpha C_\beta)$*, 8% $\delta(C_mC_\alpha N)$*, 7% $\delta(C_\alpha NC_\alpha)$*
ν_{36y}						1270	10	9	7	28	26% $\nu(C_1C_m)$, 21% $\nu(C_\alpha N)$*, 7% $\delta(C_2C_3H_p)$, 7% $\delta(C_\beta C_\beta H)$*, 7% $\nu(C_\alpha N)$
ν_{52y}					(1149)	1166	2	3	383	8	10% $\delta(C_2C_3H_p)$, 8% $\delta(C_\beta C_\beta H)$, 8% $\delta(C_\alpha C_\beta H)$, 8% $\nu(C_\alpha N)$, 7% $\nu(C_\alpha C_\beta)$
ν_{38y}	1020	3	3	−190	0	1007	1	0	−185	0	50% $\nu(C_\beta C_\beta)$*, 11% $\delta(C_\beta C_\beta H)$*
ν_{44y}						957	4	8	114	17	13% $\nu(C_\alpha N)$*, 13% $\nu(C_1C_2)$, 11% $\nu(C_\alpha C_\beta)$*, 8% $\delta(C_\alpha NH)$, 7% $\nu(C_2C_3)$
ν_{47y}						889	2	2	−52	0	33% $\delta(C_\alpha NH)$, 18% $\nu(C_\alpha C_\beta)$*, 14% $\nu(C_\alpha C_\beta)$, 12% $\nu(C_\alpha N)$
ν_{46y}						864	5	2	53	0	24% $\nu(C_\alpha C_\beta)$*, 22% $\delta(C_\alpha C_\beta C_\beta)$, 16% $\nu(C_\alpha N)$
ν_{48y}						804	4	7	44	5	13% $\delta(C_\alpha NC_\alpha)$*, 12% $\nu(C_\beta C_\beta)$*, 10% $\delta(C_\alpha C_\beta C_\beta)$, 9% $\delta(C_\beta C_\alpha N)$
ν_{49y}						453	4	1	4	2	19% $\delta(C_1C_mC_\alpha)$*, 11% $\nu(C_\alpha C_m)$, 10% $\delta(C_mC_\alpha N)$, 10% $\delta(C_1C_mC_\alpha)$
ν_{50y}						377	1	0	24	1	22% $\delta(C_\beta C_\alpha C_m)$, 14% $\delta(C_mC_\alpha N)$, 10% $\delta(C_1C_mC_\alpha)$*, 6% $\delta(C_\alpha C_mC_\alpha)$
ν_{42y}						248	0	0	2	0	22% $\delta(C_1C_mC_\alpha)$, 12% $\delta(C_\beta C_\alpha C_m)$*, 9% $\delta(C_1C_mC_\alpha)$*, 8% $\nu(C_\alpha C_m)$*
ν_{53y}						226	0	0	5	4	13% $\nu(C_1C_m)$, 8% $\delta(C_mC_\alpha N)$*, 7% $\delta(C_mC_\alpha N)$, 7% $\delta(C_\beta C_\alpha C_m)$, 7% $\delta(C_\alpha C_mC_\alpha)$
						B_{3u} Skeletal Modes					
ν_{N-Hx}						3383	9	0	0	0	99% ν(N−H)
ν_{43x}						3099	0	0	778	0	98% $\nu(C_\beta-H)$
ν_{45x}						2869	0	0	761	0	99% $\nu(C_\beta-H)$*
ν_{37x}				(1572)	(1574)	1576	0	29	4	−2	47% $\nu(C_\alpha C_m)$, 32% $\nu(C_\alpha C_m)$*, 6% $\nu(C_\beta C_\beta)$
ν_{38x}	1511	4	10	27	3	1515	0	4	33	1	51% $\nu(C_\beta C_\beta)$, 13% $\nu(C_\alpha C_m)$, 9% $\delta(C_\alpha C_\beta H)$, 9% $\nu(C_\alpha C_\beta)$, 8% $\delta(C_\beta C_\alpha N)$
ν_{39x}	1420	0	4			1424	1	16	6	−14	36% $\nu(C_\alpha C_m)$*, 12% $\nu(C_\beta C_\beta)$, 12% $\nu(C_1C_m)$, 10% $\nu(C_\alpha N)$*, 8% $\nu(C_\alpha N)$
ν_{41x}	1344	5	1	9	14	1320	7	1	4	2	25% $\nu(C_\alpha C_\beta)$, 21% $\nu(C_\alpha N)$*, 17% $\nu(C_\alpha N)$, 9% $\delta(C_mC_\alpha N)$, 9% $\delta(C_\alpha NC_\alpha)$
ν_{36x}	1266	3	8	−13	3	1264	9	5	−31	11	43% $\nu(C_\alpha N)$*, 14% $\nu(C_1C_m)$, 8% $\nu(C_\alpha C_\beta)$*
ν_{40x}	1244	5	1	−8	8	1227	3	4	−15	30	20% $\nu(C_\alpha N)$, 17% $\nu(C_1C_m)$, 10% $\nu(C_\alpha C_\beta)$*, 7% $\delta(C_2C_3H_p)$, 6% $\nu(C_\alpha N)$*
ν_{51x}						1074	0	1	308	5	37% $\delta(C_\beta C_\beta H)$, 28% $\delta(C_\alpha C_\beta H)$, 6% $\nu(C_\beta C_\beta)$
ν_{47x}						1025	6	4	6	10	12% $\delta(C_1C_2C_3)$, 11% $\delta(C_2C_3C_4)$, 10% $\nu(C_\alpha N)$*, 8% $\nu(C_\alpha C_\beta)$*, 6% $\nu(C_3C_4)$
ν_{44x}	981	9	7	12	5	986	8	3	45	0	22% $\nu(C_\alpha C_\beta)$, 12% $\nu(C_\alpha N)$, 8% $\nu(C_2C_3)$, 8% $\nu(C_1C_2)$, 7% $\nu(C_3C_4)$
ν_{48x}						864	4	6	42	−2	11% $\delta(C_\beta C_\alpha N)$, 10% $\nu(C_\alpha C_\beta)$, 9% $\delta(C_\alpha C_\beta C_\beta)$*, 9% $\nu(C_\alpha C_\beta)$*,8% δ $(C_\alpha NC_\alpha)$
ν_{46x}						743	3	7	24	0	31% $\delta(C_\alpha C_\beta C_\beta)$*, 13% $\delta(C_\beta C_\alpha N)$*, 9% $\delta(C_1C_mC_\alpha)$, 7% $\nu(C_\alpha N)$*
ν_{49x}						460	4	2	6	3	13% $\delta(C_1C_mC_\alpha)$, 12% $\delta(C_mC_\alpha N)$, 10% $\delta(C_1C_mC_\alpha)$*, 7% $\nu(C_\alpha C_m)$*
ν_{50x}						350	1	0	22	1	20% $\delta(C_\beta C_\alpha C_m)$*, 12% $\delta(C_1C_mC_\alpha)$, 9% $\delta(C_mC_\alpha N)$*, 8% $\delta(C_\beta C_\alpha N)$*
ν_{42x}						256	1	0	1	0	25% $\delta(C_1C_mC_\alpha)$*, 14% $\delta(C_\beta C_\alpha C_m)$, 10% $\delta(C_mC_\alpha N)$*, 7% $\delta(C_mC_\alpha N)$
ν_{53x}						219	0	0	6	4	12% $\nu(C_1C_m)$, 11% $\nu(C_\alpha C_m)$, 7% $\nu(C_\alpha N)$, 6% $\delta(C_mC_\alpha N)$*, 6% $\delta(C_mC_\alpha N)$

[a] The asterisk indicates atoms located at or adjacent to pyrroline rings. [b] Observed only in the 520.8-nm excitation RR spectra (not shown).

TABLE 4: Observed and Calculated Pyrroline $\delta(C_\beta H)$ and Pyrrole δ(NH) Mode Frequencies (cm^{-1}) for H_2TPBC[a]

mode	obsd N.A.	obsd $\Delta^{15}N$	obsd $\Delta^{13}C$	obsd ΔD_8	obsd ΔD_{20}	calcd N.A.	calcd $\Delta^{15}N$	calcd $\Delta^{13}C$	calcd ΔD_{12}	calcd ΔD_{20}	assignment (PED, %)
Pyrroline C_β−H Bending Modes											
A_g											
sym scissors				(1148)		1479	1	2	367	−5	25% $\delta(HC_\beta H)$*, 14% $\delta(C_\alpha C_\beta H)$*, 13% $\nu(C_\beta C_\beta)$
sym wag (ν_{17})	1278				(1284)	1267	1	2	505	2	43% $\delta(C_\beta C_\beta H)$*, 29% $\delta(C_\alpha C_\beta H)$*, 22% $\nu(C_\beta C_\beta)$*
B_{1g}											
asym scissors						1469	0	1	415	0	53% $\delta(HC_\beta H)$*, 36% $\delta(C_\alpha C_\beta H)$*, 6% $\nu(C_\alpha C_\beta)$*
asym wag (ν_{26})	1358	0	4		0	1357	1	2	356	2	54% $\delta(C_\beta C_\beta H)$*, 16% $\nu(C_\alpha C_\beta)$*, 12% $\delta(HC_\beta H)$*
B_{2g}											
asym twist	1212	0	0		0	1213	0	0	296	0	72% $\delta(C_\beta C_\beta H)$*, 27% $\delta(C_\alpha C_\beta H)$*
asym rock	1069	0	0		0	1069	0	0	227	0	72% $\delta(C_\alpha C_\beta H)$*, 23% $\delta(C_\beta C_\beta H)$*
B_{3g}											
sym twist	1216	0	0	338		1215	0	0	326	0	65% $\delta(C_\alpha C_\beta H)$*, 36% $\delta(C_\beta C_\beta H)$*
sym rock						878	0	0	218	0	59% $\delta(C_\beta C_\beta H)$*, 34% $\delta(C_\alpha C_\beta H)$*
B_{1u}											
sym twist	1213	3	4			1215	0	0	326	0	65% $\delta(C_\alpha C_\beta H)$*, 36% $\delta(C_\beta C_\beta H)$*
sym rock						878	0	0	218	0	59% $\delta(C_\beta C_\beta H)$*, 34% $\delta(C_\alpha C_\beta H)$*
B_{2u}											
sym scisssors						1474	1	5	351	−7	28% $\delta(HC_\beta H)$*, 17% $\nu(C_\alpha C_m)$, 15% $\delta(C_\alpha C_\beta H)$*, 9% $\delta(C_2C_3H_p)$
sym wag	1277	3	5	190		1278	1	3	185	0	39% $\delta(C_\beta C_\beta H)$*, 26% $\delta(C_\alpha C_\beta H)$*, 23% $\nu(C_\beta C_\beta)$*
B_{3u}											
asym scisssors						1470	0	1	428	0	52% $\delta(HC_\beta H)$*, 36% $\delta(C_\alpha C_\beta H)$*, 7% $\nu(C_\alpha C_\beta)$*
asym wag						1362	0	2	218	3	49% $\delta(C_\beta C_\beta H)$*, 16% $\nu(C_\alpha C_\beta)$*, 12%$\delta(HC_\beta H)$*
Pyrrole N−H Bending Modes											
B_{1g}											
sym δ(N−H)						1102	5	2	11	23	23% $\delta(C_\alpha NH)$, 10% $\delta(C_2C_3H_p)$, 9% $\nu(C_1C_2)$, 7% $\nu(C_\alpha C_m)$
B_{2u}											
asym δ(N−H)	1103	2	0	93	3	1107	5	1	92	17	33% $\delta(C_\alpha NH)$, 10% $\delta(C_\alpha C_\beta H)$, 9% $\nu(C_\alpha C_\beta)$

[a] The asterisk indicates atoms located at or adjacent to pyrroline rings.

the observed frequencies. In order to retain D_{2h} symmetry, the β-D_{12} isotopomer was used in the calculation, instead of the β-D_8 molecule which was actually measured. The β-D_{12} calculation provides a reasonable comparison because the C_β−H bending modes at the reduced pyrrole rings are not extensively coupled with other skeletal modes of the macrocycle.

Counting the hydrogen and phenyl C_1 atoms (Figure 1) which are bonded to the macrocycle, H_2TPBC has 42 skeletal atoms and $2n - 3 = 81$ in-plane vibrations:

$$\Gamma_{\text{in-plane}} = 19A_g + 18B_{1g} + 2B_{2g} + 2B_{3g} + 2A_u + 2B_{1u} + 18B_{2u} + 18B_{3u}$$

Seventy-nine of these modes are detectable through vibrational spectroscopy: A_g, B_{1g}, B_{2g}, and B_{3g} vibrations are Raman-active, while B_{1u}, B_{2u}, and B_{3u} vibrations are IR-active (A_u are Raman- and IR-inactive). The final force field, listed in Table 2, reproduced 79 skeletal Raman and infrared frequencies for natural abundance (NA-), [*pyrrole*-$^{15}N_4$]-, [β-D_{12}]-, [*meso*-$^{13}C_4$]-, and [*phenyl*-D_{20}]H_2TPBC. The average error for NA-H_2TPBC vibrational frequencies was 1.9 cm^{-1}, and the isotope shifts were satisfactorily calculated (Tables 3−5). Most of the skeletal modes (Table 3) are labeled according to the mode-numbering scheme developed for NiTPP.[32] Although the pyrroline C_β−H and the pyrrole N−H bending modes are also skeletal vibrations, they are tabulated separately (Table 4) for clarity. The phenyl vibrations are listed separately in Table 5. Skeletal modes are allocated to local coordinates[32] in Table 6.

Long-range interactions between $C_\alpha C_m$ bonds, *i.e.* 1,4-, 1,5-, 1,6-, and 1,9-($C_\alpha C_m$)($C_\alpha C_m$) interactions (Table 2) were required by the data. These interactions mainly affect the separation among $C_\alpha C_m$ stretching modes, *e.g.* ν_{10}, ν_{19}, ν_{37y}, and ν_{37x}. The introduction of 1,4-, 1,5-, and 1,6-($C_\alpha C_m$)($C_\alpha C_m$) interactions narrowed the separation between ν_{10} and ν_{19}, while the 1,9-($C_\alpha C_m$)($C_\alpha C_m$) interaction mainly affected the separation between Raman-active (ν_{10} and ν_{19}) and IR-active (ν_{37y} and ν_{37x}) $C_\alpha C_m$ stretching modes. Without these interactions, ν_{10} was calculated to be 60 cm^{-1} higher than ν_{19}, while ν_{37y} and ν_{37x} were calculated to be lower than ν_{10} and ν_{19}. Long-range interactions have also been introduced for free-base porphine,[33] etio-porphyrins,[35] and Ni(HOEBC).[23]

Although a single phenyl C−C force constant was used in the NiTPP calculation,[32] we scaled the three phenyl C−C stretching force constants to their bond lengths in order to fully reproduce the phenyl vibrations, especially those with symmetry of B_{1u}, B_{2g}, and B_{3g} (Table 5). For example, the calculated values for Ψ_3 and Ψ_4, 1581 and 1446 cm^{-1}, are in much better agreement with the observed frequencies (1577 and 1442 cm^{-1}) than was possible with a single C−C force constant (1600 and 1470 cm^{-1}).

C. Spectral Assignments. Figure 4 compares Soret-, Q-band-excited RR and FTIR spectra of H_2TPBC in a KBr pellet, while Soret-excited RR spectra in a KBr pellet and in THF solution are compared in Figure 5 (depolarization ratios in parentheses). Figure 6 and 7 display high-frequency (1700−900 cm^{-1}) RR spectra of H_2TPBC and its four isotopomers obtained with 363.8- and 520.8-nm excitation, and Figure 8 shows low-frequency (900−100 cm^{-1}) RR spectra obtained with 520.8-nm excitation. High-frequency FTIR spectra of the isotopomers are collected in Figure 9. Isotope shifts, selective enhancement patterns, depolarization ratios, and correspondence with NiTPP frequencies were used to assign the observed modes to the calculated vibrations. Eigenvectors of selected modes are plotted in Figure 10−12. In the following paragraphs, the modes are considered with respect to the dominant local coordinates:

C_α−C_m Stretching Modes. The eight C_α−C_m stretches divide into four in-phase (ν_{10}, ν_{19}, ν_{37y}, and ν_{37x}) and four out-of-phase modes (ν_3, ν_{28}, ν_{39y}, and ν_{39x}) which are found near 1550 and 1440 cm^{-1}, respectively. All of them have been identified *via* isotope-labeling and depolarization-ratio measurement, although ν_3 is very weak and has been seen only in the D_8 isotopomer (1402 cm^{-1}, Figure 6).

TABLE 5: Observed and Calculated Phenyl Mode Frequencies (cm^{-1}) for H_2TPBC[a]

	Phenyl Substituent Modes										
	obsd					calcd					
mode	N.A.	$\Delta^{15}N$	$\Delta^{13}C$	ΔD_8	ΔD_{20}	N.A.	$\Delta^{15}N$	$\Delta^{13}C$	ΔD_{12}	ΔD_{20}	assignment (PED, %)
A_g											
ϕ_1						3071	0	0	0	777	98% $\nu(C-H_p)$
ϕ_2						3070	0	0	0	777	98% $\nu(C-H_p)$
ϕ_3						3069	0	0	0	779	98% $\nu(C-H_p)$
ϕ_4	1599	0	0	0	32	1599	0	1	0	30	41% $\nu(C_2C_3)$, 22% $\nu(C_1C_2)$, 13% $\delta(C_1C_2H_p)$, 8% $\delta(C_2C_3H_p)$,8% $\nu(C_1C_m)$
ϕ_5	1492	1	1	6	99	1491	0	2	7	103	28% $\nu(C_\beta C_\beta)$, 16% $\delta(C_2C_3H_p)$, 13% $\nu(C_3C_4)$, 8% $\delta(C_3C_4H_p)$
ϕ_6					(838)	1176	0	1	0	329	41% $\delta(C_2C_3H_p)$, 17% $\delta(C_3C_4H_p)$, 12% $\delta(C_1C_2H_p)$, 9% $\nu(C_2C_3)$
ϕ_7						1046	0	1	0	241	29% $\nu(C_3C_4)$, 10% $\delta(C_3C_4H_p)$, 10% $\delta(C_1C_2H_p)$, 7% $\delta(C_2C_3H_p)$
ϕ_8	1003	0	−1	−1	43	1000	0	1	−3	43	15% $\delta(C_2C_3C_4)$, 15% $\delta(C_1C_2C_3)$, 9% $\delta(C_3C_4C_3)$, 9% $\nu(C_3C_4)$,8% $\delta(C_2C_1C_2)$
ϕ_9						642	0	2	1	14	21% $\delta(C_3C_4C_3)$, 12% $\delta(C_2C_1C_2)$, 11% $\delta(C_2C_3C_4)$, 7% $\nu(C_2C_3)$,6% $\nu(C_1C_2)$
ϕ_{10}	197	0	0	1	6	185	0	0	0	5	16% $\nu(C_1C_m)$, 11% $\nu(C_\alpha C_m)$, 10% $\nu(C_\alpha C_m)$*
B_{3u}											
ϕ_1'						3071	0	0	0	777	98% $\nu(C-H_p)$
ϕ_2'						3070	0	0	0	777	98% $\nu(C-H_p)$
ϕ_3'						3069	0	0	0	779	98% $\nu(C-H_p)$
ϕ_4'	1598	0	0	0	35	1599	0	1	0	33	40% $\nu(C_2C_3)$, 21% $\nu(C_1C_2)$, 13% $\delta(C_1C_2H_p)$, 8% $\delta(C_2C_3H_p)$,8% $\nu(C_1C_m)$
ϕ_5'	1487	0	−3	−12	91	1490	0	1	−7	110	27% $\delta(C_2C_3H_p)$, 21% $\nu(C_3C4)$, 13% $\delta(C_3C_4H_p)$, 9% $\nu(C_1C_2)$,7% $\nu(C_\beta C_\beta)$
ϕ_6'	1174	0	0	0		1178	0	1	0	330	42% $\delta(C_2C_3H_p)$, 17% $\delta(C_3C_4H_p)$, 14% $\delta(C_1C_2H_p)$, 8% $\nu(C_2C_3)$
ϕ_7'	1032		3	6		1051	1	1	−1	236	20% $\nu(C_3C_4)$, 9% $\delta(C_2C_3H_p)$, 9% $\nu(C_1C_2)$, 7% $\delta(C_3C_4H_p)$,6% $\delta(C_\beta C_\beta H)$
ϕ_8'	1001	0	0	0	44	997	2	1	5	48	10% $\nu(C_3C_4)$, 9% $\nu(C_2C_3)$, 8% $\delta(C_2C_3C_4)$, 8% $\delta(C_1C_2C_3)$,8% $\nu(C_\alpha C_\beta)$
ϕ_9'						672	1	1	8	18	20% $\delta(C_3C_4C_3)$, 11% $\delta(C_2C_3C_4)$, 10% $\nu(C_1C_m)$, 9% $\nu(C_1C_2)$, 8% $\delta(C_2C_1C_2)$
B_{2g}, B_{3g}, B_{1u} (Ψ, Ψ', and Ψ", respectively)											
Ψ_1						3069	0	0	0	783	98% $\nu(C-H_p)$
Ψ_1'						3069	0	0	0	783	98% $\nu(C-H_p)$
Ψ_1'						3069	0	0	0	783	98% $\nu(C-H_p)$
Ψ_2						3068	0	0	0	787	98% $\nu(C-H_p)$
Ψ_2'						3068	0	0	0	787	98% $\nu(C-H_p)$
Ψ_2'						3068	0	0	0	787	98% $\nu(C-H_p)$
Ψ_3	1577	0	0	0		1581	0	0	0	36	47% $\nu(C_1C_2)$, 34% $\nu(C_3C_4)$, 10% $\delta(C_2C_3H_p)$
Ψ_3'						1581	0	0	0	36	47% $\nu(C_1C_2)$, 34% $\nu(C_3C_4)$, 10% $\delta(C_2C_3H_p)$
Ψ_3'						1581	0	0	0	36	47% $\nu(C_1C_2)$, 34% $\nu(C_3C_4)$, 10% $\delta(C_2C_3H_p)$
Ψ_4	1442	0	0	0	124	1446	0	0	0	101	28% $\nu(C_2C_3)$, 20% $\delta(C_3C_4H_p)$, 14% $\delta(C_1C_2H_p)$, 13% $\delta(C_2C_3H_p)$, 9% $\nu(C_3C_4)$
Ψ_4'						1446	0	0	0	101	28% $\nu(C_2C_3)$, 20% $\delta(C_3C_4H_p)$, 14% $\delta(C_1C_2H_p)$, 13% $\delta(C_2C_3H_p)$, 9% $\nu(C_3C_4)$
Ψ_4'						1446	0	0	0	101	28% $\nu(C_2C_3)$, 20% $\delta(C_3C_4H_p)$, 14% $\delta(C_1C_2H_p)$, 13% $\delta(C_2C_3H_p)$, 9% $\nu(C_3C_4)$
Ψ_5				(1334)		1331	0	0	0	99	41% $\delta(C_2C_3H_p)$, 27% $\delta(C_3C_4H_p)$, 24% $\delta(C_1C_2H_p)$
Ψ_5'						1331	0	0	0	99	41% $\delta(C_2C_3H_p)$, 27% $\delta(C_3C_4H_p)$, 24% $\delta(C_1C_2H_p)$
Ψ_5'						1331	0	0	0	99	41% $\delta(C_2C_3H_p)$, 27% $\delta(C_3C_4H_p)$, 24% $\delta(C_1C_2H_p)$
Ψ_6					(1033)	1239	0	0	0	204	70% $\nu(C_3C_4)$, 49% $\nu(C_1C_2)$, 45% $\nu(C_2C_3)$
Ψ_6'						1239	0	0	0	204	70% $\nu(C_3C_4)$, 49% $\nu(C_1C_2)$, 45% $\nu(C_2C_3)$
Ψ_6'						1239	0	0	0	204	70% $\nu(C_3C_4)$, 49% $\nu(C_1C_2)$, 45% $\nu(C_2C_3)$
Ψ_7	1160	0	3	0		1157	0	0	0	320	53% $\delta(C_3C_4H_p)$, 36% $\delta(C_2C_3H_p)$
Ψ_7'						1157	0	0	0	320	53% $\delta(C_3C_4H_p)$, 36% $\delta(C_2C_3H_p)$
Ψ_7'						1157	0	0	0	320	53% $\delta(C_3C_4H_p)$, 36% $\delta(C_2C_3H_p)$
Ψ_8	1070	0	0	0		1073	0	0	0	277	44% $\delta(C_3C_4H_p)$, 33% $\nu(C_2C_3)$, 8% $\delta(C_2C_3H_p)$
Ψ_8'						1073	0	0	0	277	44% $\delta(C_3C_4H_p)$, 33% $\nu(C_2C_3)$, 8% $\delta(C_2C_3H_p)$
Ψ_8'						1073	0	0	0	277	44% $\delta(C_3C_4H_p)$, 33% $\nu(C_2C_3)$, 8% $\delta(C_2C_3H_p)$
Ψ_9	598	0	5		13	582	0	0	0	19	34% $\delta(C_2C_3C_4)$, 32% $\delta(C_1C_2C_3)$, 10% $\nu(C_3C_4)$, 9% $\nu(C_1C_2)$, 7% $\delta(C_3C_4H_p)$
Ψ_9'						582	0	0	0	19	34% $\delta(C_2C_3C_4)$, 32% $\delta(C_1C_2C_3)$, 10% $\nu(C_3C_4)$, 9% $\nu(C_1C_2)$, 7% $\delta(C_3C_4H_p)$
Ψ_9'						582	0	0	0	19	34% $\delta(C_2C_3C_4)$, 32% $\delta(C_1C_2C_3)$, 10% $\nu(C_3C_4)$, 9% $\nu(C_1C_2)$, 7% $\delta(C_3C_4H_p)$

[a] For the definition of C_1, C_2, C_3, and C_4, see Figure 1.

$C_\beta-C_\beta$ Stretching Modes. The two $C_\beta=C_\beta$ stretches give rise to a 1521-cm^{-1} RR band and a 1511-cm^{-1} IR band. The latter is assigned to ν_{38x} (B_{3u}, *x* polarized) because the $C_\beta=C_\beta$ bonds are aligned with the *x* axis, but the former can be either ν_2 or ν_{11}; ν_2 is chosen arbitrarily. The two $C_\beta-C_\beta$ single-bond stretches, ν_{11} and ν_{38y}, are observed at 1026 and 1020 cm^{-1} in the RR and FTIR spectra, respectively, and are calculated to be ~1020 cm^{-1}. Large upshifts of ν_{11} and ν_{38y} from ~1020 to ~1200 cm^{-1} upon deuteration (Figure 6 and 9) are similar to those of the C_1-C_2 stretching modes of the NiOEP ethyl groups.[36] These upshifts result from mode crossing of the $C_\beta-C_\beta$ single-bond stretching modes (Figure 10) and the symmetric pyrroline CH_2 wagging modes (Figure 11) upon deuteration of the C_β positions.

Pyrrole $C_\beta-H$, Pyrroline $C_\beta-H$, and Pyrrole N−H Bending Modes. In NiTPP, the eight $C_\beta-H$ bends give rise to four Raman modes, ν_9, ν_{17}, ν_{26}, and ν_{34}, and two (degenerate) IR modes, ν_{51} and ν_{52}.[32] In the case of H_2TPBC, four of the $C_\beta-H$ bonds are replaced by CH_2 groups, leaving two Raman and two IR $C_\beta-H$ bends: ν_9 (assigned to the 1076-cm^{-1} RR band), ν_{34} (not observed, calculated at 1146 cm^{-1}), ν_{51x} (calculated at 1074 cm^{-1}), and ν_{52y} (calculated at 1166 cm^{-1}).

The four pyrroline CH_2 groups give rise to 14 Raman and IR bending vibrations (Table 4). Like the ethyl C−H bends of NiOEP,[36] the CH_2 bends on the pyrroline rings are classified as (symmetric and asymmetric) scissoring, wagging, twisting, and rocking modes. The scissoring and the wagging modes have A_g, B_{1g}, B_{2u}, and B_{3u} symmetry, while the twisting and the rocking modes have B_{2g}, B_{3g}, A_u, and B_{1u} symmetry (A_u modes are Raman and infrared inactive). The twisting and the rocking modes do not mix with other skeletal vibrations because they are in separate symmetry blocks. However, the wagging coordinates are somewhat mixed with the pyrroline $C_\beta-C_\beta$ stretching coordinates in the ν_{11} (Figure 10 and 11) and ν_{38y} modes. This mixing is reflected in the mode-crossing phenomena upon deuteration of the C_β positions addressed above. The frequencies of these modes are very similar to the NiOEP ethyl groups, except for the asymmetric rocking mode (observed at 1069 cm^{-1}). This mode is ~300 cm^{-1} higher than that of

TABLE 6: Allocation of H_2TPBC Skeletal Mode Frequencies (cm^{-1}) to Local Coordinate[a]

local coordinate	symmetry	$A_{g\,(A1g)}$	$A_{g\,(B1g)}$	$B_{1g\,(A2g)}$	$B_{1g\,(B2g)}$	$B_{2u\,(Eu)}$	$B_{3u\,(Eu)}$
$\nu(C_1C_m)$	D_{2h}	ν_1 1226			ν_{27} 1320	ν_{36y} [1270]	ν_{36x} 1266
	D_{4h}	*1235*			*1269*		*[1254]*
$\nu(C_\alpha C_m)_{asym}$	D_{2h}		ν_{10} 1565	ν_{19} 1560		ν_{37y} 1581	ν_{37x} [1576]
	D_{4h}		*1594*	*1550*			[1586]
$\nu(C_\beta C_\beta)$	D_{2h}	ν_2 1521	ν_{11} 1026			ν_{38y} 1020	ν_{38x} 1511
	D_{4h}	*1572*	*1504*				1538
$\nu(C_\alpha C_m)_{sym}$	D_{2h}	ν_3 [1444]			ν_{28} 1421	ν_{39y} 1460	ν_{39x} 1420
	D_{4h}	*1470*			*1485*		[1473]
ν(Pyr quarter-ring)	D_{2h}			ν_{20} 1267	ν_{29} 1381	ν_{40y} 1381	ν_{40x} 1244
	D_{4h}			*1341*	*1377*		[1403]
ν(Pyr half-ring)$_{sym}$	D_{2h}	ν_4 1367	ν_{12} 1297			ν_{41y} 1365	ν_{41x} 1344
	D_{4h}	*1374*	*1302*				1308
$\delta(C_1C_m)$	D_{2h}		ν_{13} [298]	ν_{21} 307		ν_{42y} [248]	ν_{42x} [256]
	D_{4h}		*238*	*[255]*			[233]
ν(Pyr half-ring)$_{asym}$	D_{2h}			ν_{22} [1020]	ν_{30} [893]	ν_{44y} [957]	ν_{44x} 981
	D_{4h}			*1016*	*998*		1004
δ(Pyr def)$_{asym}$	D_{2h}			ν_{24} 738	ν_{32} [865]	ν_{46y} [864]	ν_{46x} [743]
	D_{4h}			*828*	*869*		[864]
ν(Pyr breathing)	D_{2h}	ν_6 995	ν_{15} 968			ν_{47y} [889]	ν_{47x} [1025]
	D_{4h}	*1004*	*1005*				[1023]
δ(Pyr def)$_{sym}$	D_{2h}	ν_7 856	ν_{16} 822			ν_{48y} [804]	ν_{48x} [864]
	D_{4h}	*889*	*846*				879
δ(Pyr rot)	D_{2h}			ν_{25} [538]	ν_{33}[376]	ν_{49y} [453]	ν_{49x} [461]
	D_{4h}			*560*	*450*		523
ν(Pyr transl)	D_{2h}	ν_8 335	ν_{18} 166			ν_{50y} [377]	ν_{50x} [350]
	D_{4h}	*402*	*277*				445
$\delta(C_\beta H)_{asym}$	D_{2h}			(asym wag 1358; ν_{26})	ν_{34}[1146]	(sym wag, 1277)	ν_{51x} [1074]
	D_{4h}			*1230*	*1190*		1071
$\delta(C_\beta H)_{sym}$	D_{2h}	ν_9 1076	(sym wag 1278; ν_{17})			ν_{52y} [1166]	(asym wag, [1362])
	D_{4h}	*1079*	*1084*				1204
δ(Pyr transl)	D_{2h}				ν_{35} [377]	ν_{53y} [226]	ν_{53x} [219]
	D_{4h}				*109*		[306]

[a] The calculated frequencies are given in square brackets. For comparison, the frequencies of metallo-TPP are also listed in *italic* font under D_{4h} symmetry (the Raman and calculated IR frequencies are from NiTPP, and the observed IR frequencies are from CuTPP).

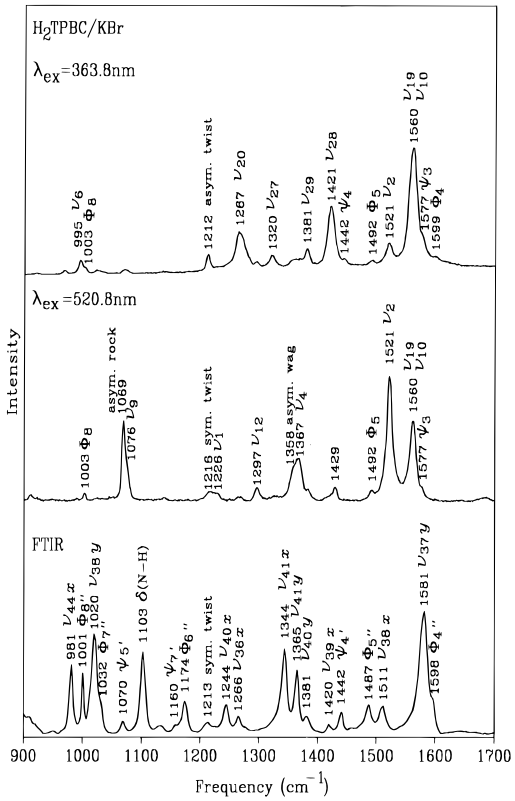

Figure 4. Soret- and Q_x-band-excited RR spectra and the FT-IR spectrum of H_2TPBC in a KBr pellet. Experimental conditions: 4-cm^{-1} spectral slit, 1-cm^{-1}/s scan rate, 3 scans for 363.8 nm at 30 mW, and 2 scans for 520.8 nm at 50 mW. FT-IR spectrum resolution: 4 cm^{-1}.

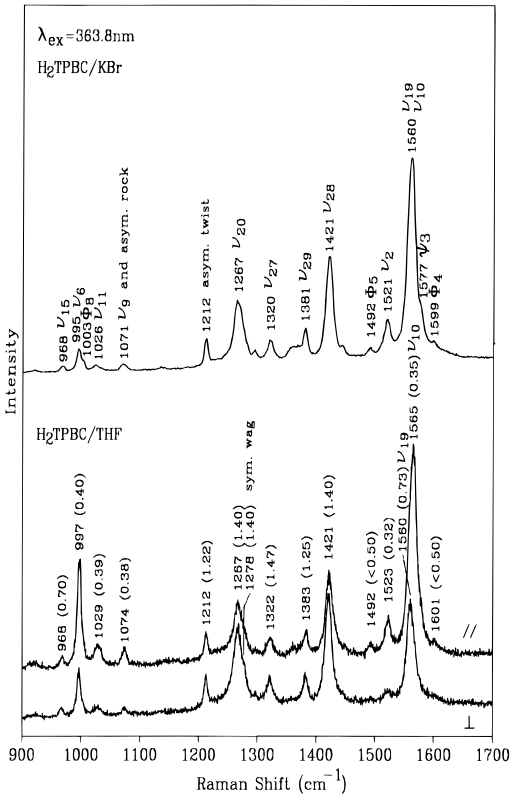

Figure 5. 363.8-nm-excited RR spectra of H_2TPBC in a KBr pellet (top) and in THF solution (bottom). Both parallel and perpendicular traces are shown for the solution RR spectrum, and the depolarization ratios are marked in parentheses. Experimental conditions: same as in Figure 4 for the KBr spectrum; for the solution spectrum, 4-cm^{-1} spectral slit, 0.5 cm^{-1}/s, 2 scans at 20 mW for 363.8 nm with the use of a cylindrical lens.

NiOEP ethyl groups[36] probably because the vibration involves conformational changes of the pyrroline rings.[37]

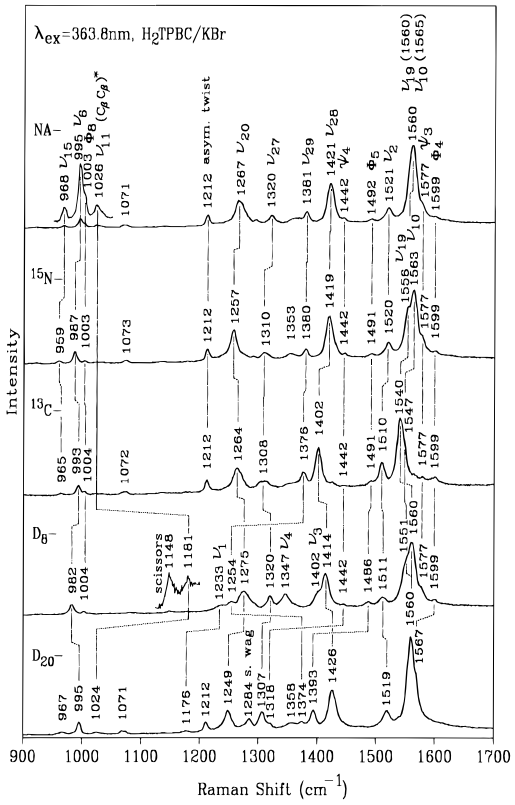

Figure 6. High-frequency Soret-excited RR spectra of natural abundance (NA-) H_2TPBC and its pyrrole-$^{15}N_4$, β-D_8, *meso*-$^{13}C_4$, and phenyl-D_{20} isotopomers. Experimental conditions are as in Figure 4.

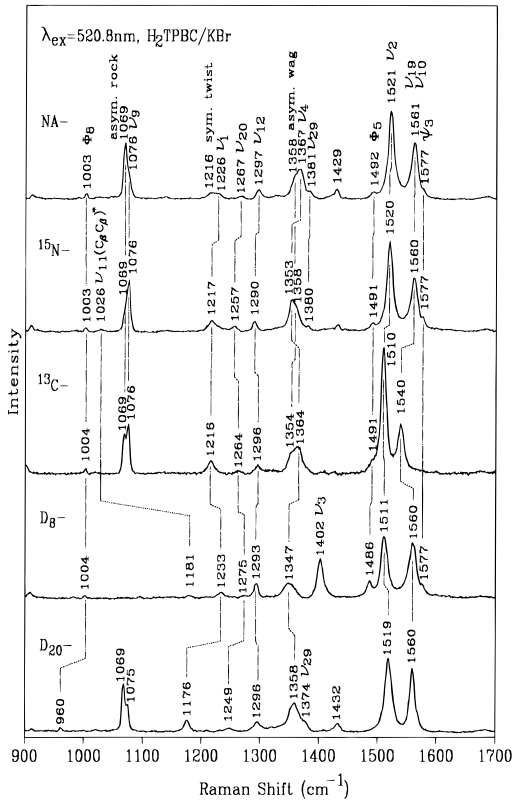

Figure 7. As in Figure 6, but with 520.8-nm excitation.

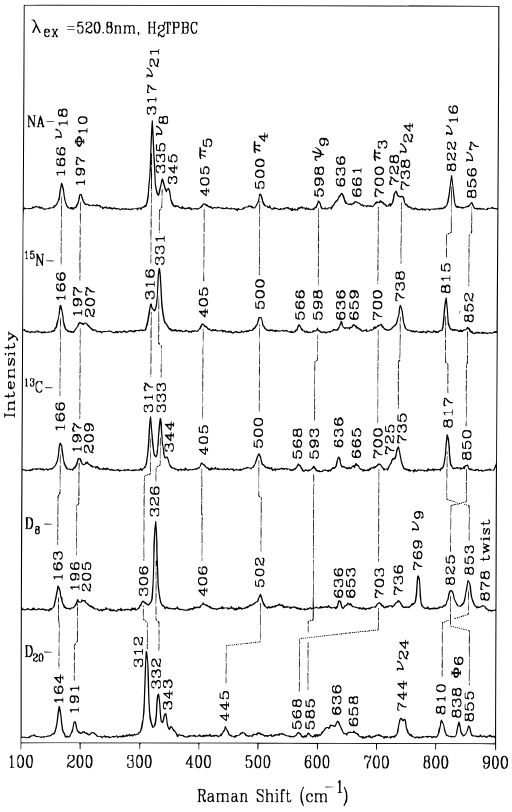

Figure 8. As in Figure 7, but in the low-frequency region.

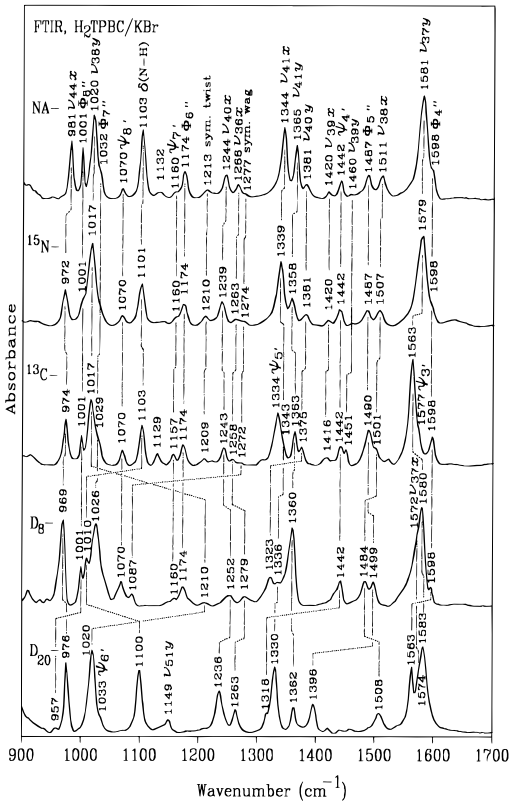

Figure 9. FT-IR spectra of NA-, [^{15}N]-, [^{13}C]-, [D_8]-, and [D_{20}]H_2-TPBC in KBr pellet at 4-cm^{-1} resolution.

There are two pyrrole (symmetric and asymmetric) N−H bending modes (Table 4). Only one mode was observed at 1103 cm^{-1} in the FTIR spectrum (Figure 9). This mode has been observed at 1209 cm^{-1} for free-base porphine.[33] Interestingly, these modes are calculated to be C_β-deuteration sensitive for H_2TPBC, and the band at 1103 cm^{-1} does shift for the D_8 isotopomer.

Low-Frequency Modes. Several RR bands were observed in the low-frequency region (Figure 8). These modes are mainly rotations and translations of the pyrrole and pyrroline rings. The pyrrole and pyrroline rotations (ν_{25}, ν_{33}, ν_{49y}, and ν_{49x}) were

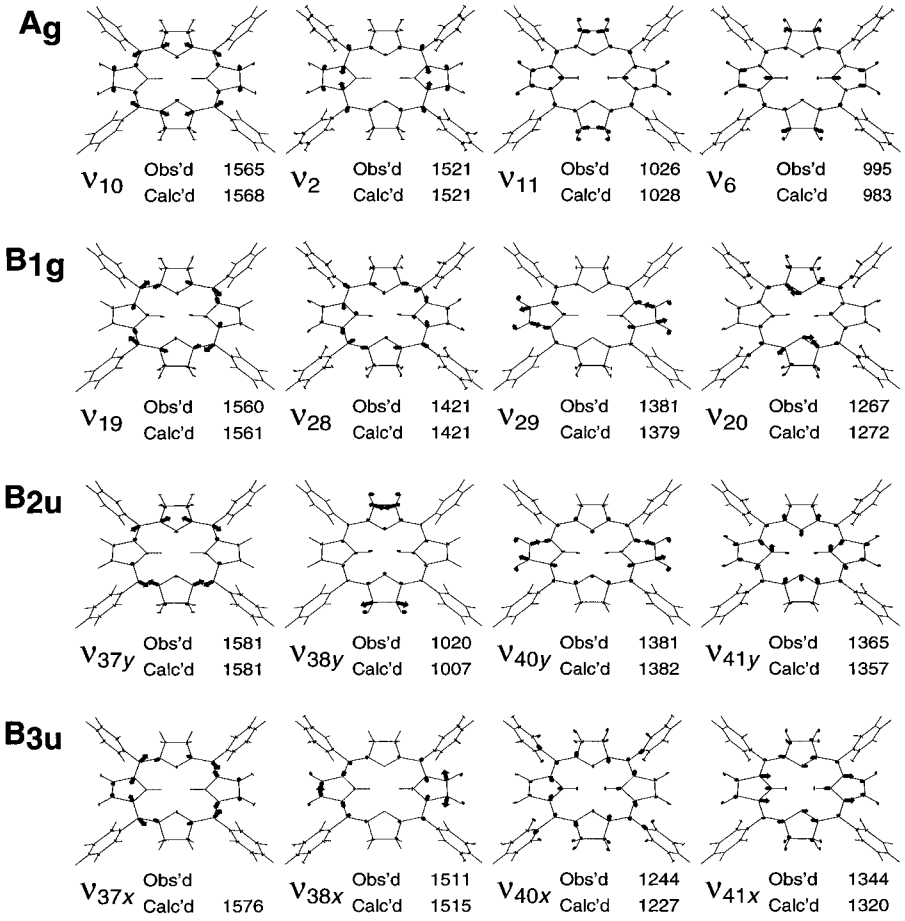

Figure 10. Eigenvector plots of selected skeletal vibrations.

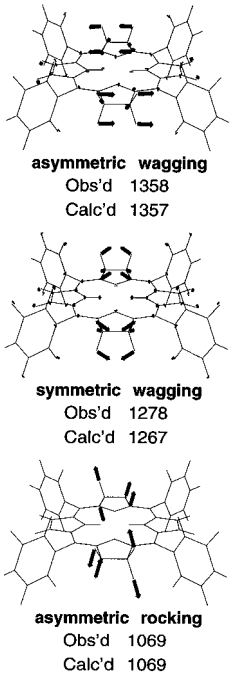

Figure 11. Eigenvector plots of three pyrroline CH_2 bending modes.

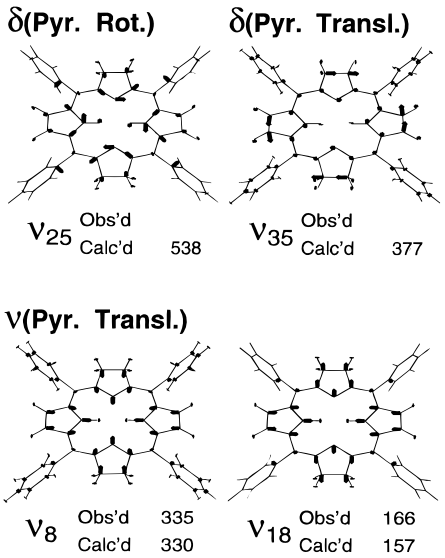

Figure 12. Eigenvector plots of four low-frequency skeletal vibrations.

observed at ~500 cm^{-1} and the translations at ~350 cm^{-1} (ν_8, ν_{18}, ν_{50y}, ν_{50x}, ν_{35}, ν_{53y}, and ν_{53x}). The eigenvector plots of four selected modes are depicted in Figure 12.

Phenyl Modes. The vibrations of the phenyl groups are not affected by the reduction of the pyrrole rings, and their frequencies and isotope shifts are very similar to those of NiTPP[32] (Table 5). The B_{1g} and B_{2u} phenyl vibrations are not listed because they are nearly identical to phenyl modes with A_g and B_{3u} symmetry, respectively.

The phenyl vibrations of B_{2g}, B_{3g}, and B_{1u} symmetry (Ψ, Ψ', and Ψ'' modes) have been reported for *mono*substituted benzenes[38] and biphenyl[31] but were not observed in the NiTPP RR spectra.[32] The respective modes in each symmetry block have exactly the same frequency, isotope shift, and potential energy distribution, but differ in phasing.

Out-of-Plane Vibrations. There are candidates for out-of-plane vibrational modes in the region from 750 to 200 cm^{-1}. The frequencies and isotope shifts of these modes are similar to the phenyl out-of-plane vibrations (π_3, π_4, and π_5) reported for NiTPP.[32]

D. Comparison with NiTPP and CuTPBC. The mode correlation with NiTPP works well, once allowance is made

for the effects of pyrrole reduction to pyrroline. Thus, four of the C_β−H bends are replaced by a set of pyrroline CH_2 modes: scissors, wags, twists, and rocks. The $C_\beta C_\beta$ stretches are now divided into double-bond (ν_2 and ν_{38x} at 1521 and 1511 cm^{-1}) and single-bond (ν_{11} and ν_{38y} at 1026 and 1020 cm^{-1}) pairs. Likewise, modes with predominant $C_\alpha C_\beta$ stretching contributions are divided into pyrrole and pyrroline pairs, although the frequencies are less widely separated, *e.g.* ν_{40y} (1381 cm^{-1}) and ν_{40x} (1244 cm^{-1}).

However, the eigenvectors of the modes primarily involving the $C_\alpha C_m$ and $C_\alpha N$ bonds of the 16-membered inner ring are essentially unaltered from NiTPP (Figure 10). For example, the $(C_\alpha C_m)_{asym}$ Raman modes, ν_{10} (A_g) and ν_{19} (B_{1g}), look very much like their B_{1g} and A_{2g} parents in NiTPP. So too do their IR counterparts, ν_{37x} and ν_{37y}, which resemble degenerate components of the E_u parent; indeed the degeneracy is split by only 5 cm^{-1}. The bond distances of adjacent $C_\alpha C_m$ bonds differ by 0.02 Å, and the force constants differ by 0.4 mdyn/Å (Tables 1 and 2), but these differences do not produce mode localization. The eigenvectors show little tendency to segregate on the basis of long *vs* short $C_\alpha C_m$ bonds. This is true also for the modes involving large $C_\alpha N$ contributions. These modes also resemble the NiTPP counterparts. We note that Donohoe *et al.*[18b] did report localization of $C_\alpha C_m$ and $C_\alpha N$ modes in CuTPBC, using a different empirical force field. The reason for this variance in mode characters is unclear.

The absence of a metal ion at the center of the ring also has little influence on the eigenvectors, but some frequencies are lowered significantly. Thus, the ν_2 and ν_{10} frequencies are 20−30 cm^{-1} lower in H_2TPBC (1521 and 1562 cm^{-1}) than in CuTPBC[18b] (1543 and 1598 cm^{-1}). Parallel increases have been observed between H_2TPP (1555 and 1556 cm^{-1}) and NiTPP (1572 and 1594 cm^{-1}) and between free-base (1546 and 1610 cm^{-1}) and nickel porphine (1574 and 1650 cm^{-1}).

As might be expected, the pyrrole translational modes are also affected. ν_8 and ν_{18} are 335 and 116 cm^{-1} for H_2TPBC, but 385 and 202 cm^{-1} for CuTPBC. The binding of Cu at the center of the ring adds Cu−N stretching character to these modes.

E. RR Enhancement Pattern. Although the crystal structure of (Py)ZnTPBC shows a slightly buckled conformation,[27] the mutual exclusion rule holds well for H_2TPBC (Figure 4): vibrational modes found in RR spectra were not observed in the FTIR spectrum, and *vice versa*. This evidence for an inversion center justifies the assumption made in the normal mode calculation that H_2TPBC has effective D_{2h} symmetry.

The symmetry correlation between the D_{4h} and D_{2h} point group is given in Table 7, along with the Raman depolarization ratios and the directions of IR polarizations. As a result of symmetry lowering, A_{1g} and B_{1g} (under D_{4h}) merge to A_g (under D_{2h}), A_{2g} and B_{2g} merge to B_{1g}, and E_g (E_u) splits into B_{2g} and B_{3g} (B_{2u} and B_{3u}). The H_2TPBC spectra are consistent with these symmetry properties. As seen in Figure 5, the depolarization ratio is <0.75 for A_g modes (ν_{10}, ν_2, ν_9, ν_{11}, ν_6, and ν_{15}), and >0.75 for the B_{1g} modes (ν_{28}, ν_{29}, ν_{27}, and ν_{20}).

There is an interesting reversal in the RR enhancement pattern for H_2TPBC, relative to porphyrins. RR spectra of porphyrins are dominated by totally symmetric modes when excited in the B band, but non-totally symmetric modes when excited in the Q bands.[32,36] The weakness of the Q transition moment resulting from the configuration interaction allows vibronic (B-term) scattering to dominate, whereas Frank−Condon (A-term) scattering dominates in resonance with the allowed Soret transition. The lifting of configuration in H_2TPBC induces large Q transition moments and allows the dominance of totally symmetric modes (ν_{10}, ν_2, ν_4, and ν_9—see Figure 4) *via* Frank−Condon scattering with 520.8-nm excitation; the non-totally symmetric modes are weak. In contrast, the non-totally symmetric modes (ν_{19}, ν_{28}, and ν_{20}) are quite strong with 363.8-nm excitation (Figure 5), being exceeded only by ν_{10}. These bands arise from vibronic scattering, which must result from vibronic mixing of the close-lying B_x (378 nm) and B_y (356 nm) transitions (Figure 2). Similar evidence for B_x/B_y vibronic mixing was found for the C_β-ethyl-substituted bacteriochlorin, Ni(HOEBC).[23] Thus vibronic scattering is seen with Q excitation in porphyrins, as a result of Q forbiddenness and Q/B mixing, but with B excitation in bacteriochlorin, as a result of the close spacing and mixing of the B_x and B_y transitions.

TABLE 7: Symmetry Correlation between D_{4h} and D_{2h} Groups

D_{4h}	ρ[a]	D_{2h}	ρ
A_{1g}	1/8	A_g	1/8 - 3/4
B_{1g}	3/4		
A_{2g}	∞	B_{1g}	3/4 - ∞
B_{2g}	3/4		
E_g	3/4 - ∞	B_{2g}	3/4 - ∞
		B_{3g}	3/4 - ∞
A_{2u}	*z*	B_{1u}	*z*
E_u	*x*, *y*	B_{2u}	*y*
		B_{3u}	*x*

[a] The depolarization ratios are given for Raman active modes, while the directions of polarization are given for IR active modes.

There is also evidence for RR mode selectivity *via* the transition-moment direction in H_2TPBC. For example, ν_2 is the strongest band in the 520.8-nm-excited spectrum but ν_6 is unobservable, while the two modes have comparable intensity with 363.8-nm excitation (Figure 2). The eigenvectors (Figure 10) show bond stretching mostly in the *x* direction for ν_2 and the *y* direction for ν_6. It is reasonable to suppose that the excited state displacement in the Q_x state is large for ν_2 (large α_{xx}' tensor element) but small for ν_6, accounting for the intensity disparity with 520.8-nm excitation. A reversal would be expected for the Q_y state, but Q_y-excited RR spectra are unobtainable because of intrinsic fluorescence. The comparable ν_2 and ν_6 intensities observed with 363.8-nm excitation are attributable to this wavelength lying between the B_x and B_y transitions; B_x is expected to enhance ν_2, while B_y is expected to enhance ν_6. Similar directional selectivity was reported for CuTPBC by Donohoe *et al.*,[18b] who were able to demonstrate the effect with Q_y excitation since fluorescence is quenched by the Cu^{2+}.

Acknowledgment. We thank Dr. Songhzou Hu for helpful discussions on the synthesis and the normal mode calculation. This work was supported by DOE Grant DE-F G02-93ER-14403.

References and Notes

(1) Scheer, H., Ed. *Chlorophylls*; CRC: Boca Raton, FL, 1991.

(2) For brief introductions, see: (a) Barber, J.; Andersson, B. *Nature* **1994**, *370*, 31−34. (b) Fleming G. R.; van Grondelle R. *Phys. Today* **1994**, *47* (Feb), 48−55. (c) Norris, J. R.; Schiffer, M. *Chem. Eng.* **1990**, *68* (July 30), 22−37.

(3) (a) Deisenhofer, J.; Epp, O.; Miki, K.; Huber, R.; Michel, H. *J. Mol. Biol.* **1984**, *180*, 385−398. (b) Deisenhofer, J.; Epp, O.; Miki, K.; Huber, R.; Michel, H. *Nature* **1985**, *318*, 618−624.

(4) (a) Allen, J. P.; Feher, G; Yeates, T. O.; Komiya, H.; Rees, D. C. *Proc. Natl. Acad. Sci. U.S.A.* **1987**, *84*, 5730−5734. (b) 6162−6166. (c) Yeates, T. O.; Komiya, H.; Rees, D. C.; Allen, J. P.; Feher, G. *Proc. Natl. Acad. Sci. U.S.A.* **1987**, *84*, 6438−6442. (d) Allen, J. P.; Feher, G; Yeates, T. O.; Komiya, H.; Rees, D. C. *Proc. Natl. Acad. Sci. U.S.A.* **1988**, *85*, 8487−8491.

(5) McDermott, G.; Prince, S. M.; Freer, A. A.; Hawthornthwaite-Lawless, A. M.; Papiz, M. Z.; Cogdell, R. J.; Isaacs, N. W. *Nature* **1995**, *374*, 517−521.

(6) (a) Fajer, J.; Borg, D. C.; Forman, A.; Dolphin, D.; Felton, R. H. *J. Am. Chem. Soc.* **1973**, *95*, 2739−2741. (b) Fajer, J.; Borg, D. C.; Forman, A.; Felton, R. H.; Dolphin, D.; Vegh, L. *Proc. Natl. Acad. Sci. U.S.A.* **1974**, *71*, 994−998. (c) Fajer, J.; Forman, A.; Davis, M. S.; Spaulding, L. D.; Brune, D. C.; Felton, R. H. *J. Am. Chem. Soc.* **1977**, *99*, 4134−4140. (d) Davis, M. S.; Forman, A.; Hanson, L. K.; Thornber, J. P.; Fajer, J. *J. Phys. Chem.* **1979**, *83*, 3325−3332. (e) Fajer, J.; Fujita, E.; Forman, A.; Hanson, L. K.; Craig, G. W.; Goff, D. A.; Kehres, L. A.; Smith, K. M. *J. Am. Chem. Soc.* **1983**, *105*, 3837−3843. (f) Horning, T. L.; Fujita, E.; Fajer, J. *J. Am. Chem. Soc.* **1986**, *108*, 323−325.

(7) (a) Lubitz, W.; Lendzian, F.; Möbius, K. *Chem. Phys. Lett.* **1981**, *81*, 235−241. (b) Lendzian, F.; Möbius, K.; Plato, M.; Smith, U. H.; Thrunauer, M. C.; Lubitz, W. *Chem. Phys. Lett.* **1984**, *111*, 583−588. (c) Lubitz, W.; Isaacson, R. A.; Abresch, E. C.; Feher, G. *Proc. Natl. Acad. Sci. U.S.A.* **1984**, *81*, 7792−7796. (d) Käss, H.; Rantter, J.; Zweygart, W.; Struch, A.; Scheer, H.; Lubitz, W. *J. Phys. Chem.* **1994**, *98*, 354−363.

(8) Mäntele, W.; Wollenweber, A.; Rashwan, F.; Heinze, J.; Nabedryk E.; Berger, G.; Breton, J. *Photochem. Photobiol.* **1988**, *47*, 451−455.

(9) Spiro, T. G. Ed. *Biological Applications of Raman Spectroscopy*; Wiley: New York, 1988; Vol. III.

(10) Hirschfeld, T.; Chase, B. *Appl. Spectrosc.* **1986**, *40*, 133−137. (b) Schrader, B.; Hoffmann, A.; Simon, A.; Podschadlowski, R.; Tischer, M. *J. Mol. Struct.* **1990**, *217*, 207−220.

(11) (a) Lutz, M., Kleo, J. *Biochem. Biophys. Res. Commun.* **1976**, *69*, 711−717. (b) Lutz, M.; Kleo, J. *Biochim. Biophys. Acta* **1979**, *546*, 365−369. (c) Lutz, M.; Hoff, A.; Brehamet, L. *Biochim. Biophys. Acta* **1982**, *679*, 331−341. (d) Cotton, T. M.; Van Duyne *Biochem. Biophys. Res. Commun.* **1978**, *82*, 424−433. (e) Cotton, T. M.; Parks, K. D.; Van Duyne, R. P. *J. Am. Chem. Soc.* **1980**, *102*, 6399−6407. (f) Cotton, T. M.; Van Duyne, R. P. *J. Am. Chem. Soc.* **1981**, *103*, 6020−6026. (g) Callahan, P. M.; Cotton, T. M. *J. Am. Chem. Soc.* **1987**, *109*, 7001−7007. (h) Donohoe, R. J.; Frank, H. A.; Bocian, D. F. *Photochem. Photobiol.* **1988**, *48*, 531−537. (i) Nishizawa, E.; Koyama, Y. *Chem. Phys. Lett.* **1990**, *172*, 317−322. (j) Nishizawa, E.; Koyama, Y. *Chem. Phys. Lett.* **1991**, *176*, 390−394. (k) Peloquin, J. M.; Bylina, E. J.; Youvan, D. C.; Bocian, D. F. *Biochemistry* **1990**, *29*, 8417−8424. (l) Palaniappan, V.; Martin, P. C.; Chynwat, V.; Frank, H. A.; Bocian, D. F. *J. Am. Chem. Soc.* **1993**, *115*, 12035−12049. (m) Diers, J. R.; Bocian, D. F. *J. Phys. Chem.* **1994**, *98*, 12884−12892. (n) Palaniappan, V.; Bocian, D. F. *Biochemistry* **1995**, *34*, 11106−11116.

(12) (a) Donohoe, R. J.; Dyer, R. B; Swanson, B. I.; Violette, C. A.; Frank, H. A.; Bocian, D. F. *J. Am. Chem. Soc.* **1990**, *112*, 6716−6718. (b) Shreve, A. P.; Cherepy, N. J.; Franzen, S.; Boxer, S. G.; Mathies, R. A. *Proc. Natl. Acad. Sci. U.S.A.* **1991**, *88*, 11207−11211. (c) Palaniappan, V.; Aldema, M. A.; Frank, H. A.; Bocian, D. F. *Biochemistry* **1992**, *31*, 11050−11058. (d) Feiler, U.; Albouy, D.; Pourcet, C.; Mattioli, T. A.; Lutz, M.; Robert, B. *Biochemistry* **1994**, *33*, 7594−7599. (e) Cherepy, N. J.; Shreve, A. P.; Moore, L. J.; Franzen S.; Boxer, S. G.; Mathies, R. A. *J. Phys. Chem.* **1994**, *98*, 6023−6029. (f) Diers, J. R.; Bocian, D. F. *J. Am. Chem. Soc.* **1995**, *117*, 6629−6630. (g) Palaniappan V.; Schenck, C. C.; Bocian, D. F. *J. Phys. Chem.* **1995**, *99*, 17049−17058. (h) Cherepy N. J.; Holzwarth, A. R.; Mathies, R. A. *Biochemistry* **1995**, *34*, 5288−5293. (I) Diers, J. R.; Zhu, Y.; Blankenship, R. E.; Bocian, D. F. *J. Phys. Chem.* **1996**, *100*, 8573−8579.

(13) (a) Johnson, C. K.; Rubinovitz, R.; *Spectrochim. Acta* **1991**, *47A*, 1413−1421. (b) Noguchi, T.; Furukawa, Y.; Tasumi, M. *Spectrochim. Acta* **1991**, *47A*, 1431−1440. (c) Mattioli, T. A.; Hoffmann, A.; Robert, B.; Schrader, B.; Lutz, M. *Biochemistry* **1991**, *30*, 4648−4654. (d) Okada, K.; Nishizawa, E.; Fujimoto, Y.; Koyama, Y.; Muraishi, S.; Ozaki, Y. *Appl. Spectrosc.* **1992**, *46*, 518−523. (e) Wachtveitl, J.; Farchaus, J. W.; Das, R.; Lutz, M.; Robert, B.; Mattioli, T. A. *Biochemistry* **1993**, *32*, 12875−12886. (f) Mattioli, T. A.; Lin, X.; Allen, J. P.; Williams, J. C. *Biochemistry* **1995**, *34*, 6142−6152. (g) Sato, H.; Uehara, K.; Ishii, T.; Ozaki, Y. *Biochemistry* **1995**, *34*, 7854−7860. (h) Sturgis, J. N.; Hagemann, G.; Tadros, M. H.; Robert, B. *Biochemistry* **1995**, *34*, 10519−10524. (i) Sturgis, J. N.; Jirsakova, V.; Reiss-Husson, F.; Cogdell, R. J.; Robert, B. *Biochemistry* **1995**, *34*, 517−523. (j) Feiler, U.; Albouy, D.; Robert, B. Mattioli, T. A. *Biochemistry* **1995**, *34*, 11099−11105. (k) Goldsmith, J. O.; King, B.; Boxer, S. G. *Biochemistry* **1996**, *35*, 2421−2428. (l) Ivancich, A.; Feick, R.; Ertlmaier, A.; Mattioli, T. A. *Biochemistry* **1996**, *35*, 6126−6135. (m) Allen, J. P.; Artz, K.; Lin, X.; Williams, J. C.; Ivancich, A.; Albouy, D.; Mattioli, T. A.; Fetsch, A.; Kuhn, M.; Lubitz, W. *Biochemistry* **1996**, *35*, 6612−6619.

(14) (a) Andersson, L. A.; Loehr, T. M.; Lim, A. R.; Mauk, A. G. *J. Biol. Chem.* **1984**, *259*, 15340. (b) Andersson, L. A.; Loehr, T. M.; Chang, C. K.; Mauk, A. G. *J. Am. Chem. Soc.* **1985**, *107*, 182. (c) Andersson, L. A.; Loehr, T. M.; Sotiriou, C.; Wu, W.; Chang, C. K. *J. Am. Chem. Soc.* **1986**, *108*, 2908. (d) Andersson, L. A.; Sotiriou, C.; Chang, C. K.; Loehr, T. M. *J. Am. Chem. Soc.* **1987**, *109*, 258. (e) Andersson, L. A.; Loehr, T. M.; Stershic, M. T.; Stolzenberg, A. M. *Inorg. Chem.* **1990**, *29*, 2278. (f) Andersson, L. A.; Loehr, T. M.; Thompson, R. G.; Strauss, S. H. *Inorg. Chem.* **1990**, *29*, 2142.

(15) (a) Ozaki, Y.; Kitagawa, T.; Ogoshi, H. *Inorg. Chem.* **1979**, *18*, 1772. (b) Ozaki, Y.; Iriyama, K.; Ogoshi, H.; Ochiai, T.; Kitagawa, T. *J. Phys. Chem.* **1986**, *90*, 6105.

(16) (a) Salehi, A.; Oertling, W. A.; Fonda, H. N.; Babcock, G. T.; Chang, C. K. *Photochem. Photobiol.* **1988**, *48*, 525−530. (b) Fonda, H. N.; Oertling, W. A.; Salehi, A.; Chang, C. K.; Babcock, G. T. *J. Am. Chem. Soc.* **1990**, *112*, 9497−9507.

(17) Prendergast, K.; Spiro, T. G. *J. Phys. Chem.* **1991**, *95*, 1555−1563;

(18) (a) Boldt, N. J.; Donohoe, R. J.; Birge, R. R.; Bocian, D. F. *J. Am. Chem. Soc.* **1987**, *109*, 2284. (b) Donohoe, R. J.; Atamian, M.; Bocian, D. F. *J. Phys. Chem.* **1989**, *93*, 2244−2252. (c) Procyk, A. D.; Kim, Y.; Schmidt, E.; Fonda, H. N.; Chang, C. K.; Babcock, G. T.; Bocian, D. F. *J. Am. Chem. Soc.* **1992**, *114*, 6539−6549.

(19) Gladkov, L. L.; Starukhin, A. S.; Shulga, A. M. *Spectrochim. Acta* **1987**, *43A*, 1125.

(20) (a) Cotton, T. M.; Timkovich, R.; Cork, M. S. *FEBS Lett.* **1981**, 133, 39−44. (b) Ching, Y.; Ondrias, M. R.; Rousseau, D. L.; Muhoberac, B. B.; Wharton, D. C. *FEBS Lett.* **1982**, *138*, 239−244. (c) Ondrias, M. R.; Carson, S. D.; Hirasawa, M.; Knaff, D. B. *Biochim. Biophys. Acta* **1985**, *830*, 159−163. (d) Han, S.; Madden, J. F.; Thompson, R. G.; Strauss, S. H.; Siegel, L. M.; Spiro, T. G. *Biochemistry* **1989**, *28*, 5461−5470. (d) Andersson, L. A.; Loehr, T. M.; Wu, W.; Chang, C. K.; Timkovich, R. *FEBS Lett.* **1990**, *267*, 285−288. (e) Andersson, L. A.; Loehr, T. M.; Thompson, R. G.; Strauss, S. H. *Inorg. Chem.* **1990**, *29*, 2142. (f) Lai, K. K.; Yue, K. T. *J. Raman Spectrosc.* **1990**, *21*, 21−26.

(21) Melamed, D.; Sullivan, E. P.; Prendergast, K.; Strauss, S. H.; Spiro, T. G. *Inorg. Chem.* **1991**, *30*, 1308−1319.

(22) Procyk, A. D.; Bocian, D. F. *J. Am. Chem. Soc.* **1991**, *113*, 3765−3773.

(23) Hu, S.; Mukherjee, A.; Spiro, T. G. *J. Am. Chem. Soc.* **1993**, *115*, 12366−12377.

(24) Whitlock, Jr., H. W.; Hanauer, R.; Oester, M. Y.; Bower, B. K. *J. Am. Chem. Soc.* **1969**, *91*, 7485−7489.

(25) Lindsey, J. S.; Schreiman, I. C.; Hsu, H. C.; Kearney, P. C.; Marguerettaz, A. M. *J. Org. Chem.* **1987**, *52*, 827−836.

(26) Wilson, E. B.; Decius, J. C.; Cross, P. C. *Molecular Vibrations*; McGraw-Hill: New York, 1955.

(27) Barkigia, K. M.; Miura, M.; Thompson, M. A.; Fajer, J. *Inorg. Chem.* **1991**, *30*, 2233−2236.

(28) Mukherjee, A.; Spiro, T. G. *QCPE Bull.* **1995**, *15* (1), Program 656.

(29) (a) Gouterman, M. *J. Chem. Phys.* **1959**, *30*, 1139−1161. (b) Goutermen, M. *J. Mol. Spectrosc.* **1961**, *3*, 138−163. (c) Gouterman, M.; Eagnière, G. H., Snyder, L. C. *J. Mol. Spectrosc.* **1963**, *11*, 108−127. (d) Weiss, C.; Kobayashi, H.; Gouterman, M. *J. Mol. Spectrosc.* **1965**, *16*, 415−450.

(30) Hargreaves, A.; Rizvi, S. H. *Acta Crystallogr.* **1962**, *15*, 365−373.

(31) Zerbi, G.; Sandroni, S. *Spectrochim. Acta* **1968**, *24A*, 511−528.

(32) Li, X.-Y.; Czernuszewicz, R. S.; Kincaid, J. R.; Stein, P.; Spiro, T. G. *J. Phys. Chem.* **1990**, *94*, 31−47.

(33) Li, X.-Y.; Zgierski, M. Z. J. *Phys. Chem.* **1991**, *95*, 4268,-4287.

(34) Burgi, H.; Dunitz, J. D. *J. Am. Chem. Soc.* **1987**, *109*, 2924−2927.

(35) Hu, S.; Mukherjee, A.; Piffat, C.; Mak, R. S. W.; Li, X.-Y.; Spiro, T. G. *Biospectroscopy* **1995**, *1*, 395−412.

(36) Li, X.-Y.; Czernuszewicz, R. S.; Kincaid, J. R.; Stein, P.; Spiro, T. G. *J. Phys. Chem.* **1990**, *94*, 47−61.

(37) The asymmetric rocking mode involves pseudorotation of the pyrroline $C_\beta-C_\beta$ single bond and changes the pyrroline rings from one *envelop* conformation to another *via* an *eclipsed* conformation in which the ring atoms are all in-plane. This *eclipsed* conformation results in different bond angles of the (sp^3) CH_2 groups from 109.5° (tetrahedral bond angle) and creates instability of the pyrroline rings. The elevated frequency of the asymmetric rocking mode is attributed to the high-energy state of the *eclipsed* conformation. To fit the frequency, the $H(C_\alpha C_\beta H)$ and $H(C_\beta C_\beta H)$ force constants were elevated to ∼0.7 mdyn/rad^2 (Table 2) from the ethyl value, 0.625 mdyn/rad^2.

(38) Green, J. H. S. *Spectrochim Acta.* **1961**, *17*, 607−613.